Bi-Annual

ISSN 1665-8607

QUAID-E-AWAM UNIVERSITY RESEARCH JOURNAL OF ENGINEERING, SCIENCE & TECHNOLOGY

VOLUME 7 NO. 1 JAN-JUN 2006

QUAID-E-AWAM UNIVERSITY OF ENGINEERING SCIENCE & TECHNOLOGY
NAWABSHAH-67480 SINDH PAKISTAN ISSN: 1665-8607

Professor Dr. Saleem Raza Samo
Editor
Phone: +92-244-9370361 Fax: +92-244-9370362
E-Mail: srsamo@yahoo.com

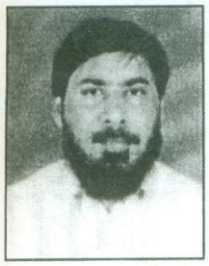

FROM THE EDITOR'S DESK

Dear Researchers/Readers

Aslam-o-Alaikum

God Almighty is worthy of all acknowledgements. The editorial board thankfully acknowledges the support and cooperation of the individuals who have contributed in this issue. It is our topmost priority to publish quality research papers in QUEST research journal. Ofcourse! it is quite tough task to achieve this goal and we are struggling hard to present you the best to read. We are confident that QUEST journal is one of the premier research journals published in this region.

It has been a continuous effort to search and bring the best research work carried out not only in QUEST, but also in other reputable national and international institutions. In this issue, which you are holding in your hands, you will find the quality research work carried out not only in this country but also in other countries. We hope you will find this issue quite informative and useful. Your valuable comments and suggestions for improvements are always welcome.

May God Almighty give the ability and strength to serve the humanity and be kind to His creation.

Best Regards.

Prof. Dr Saleem Raza Samo
Editor-in-Chief
QURJEST

CO-FIRING OF COMMERCIAL FUEL OIL AND PRODUCER GAS FROM DOWNDRAFT GASIFIER FOR INDUSTRIAL APPLICATIONS

Ahmad Hussain*, Saleem Raza Samo** and Farid Nasir Ani***

ABSTRACT

Biomass is one of the most promising energy resource which is expected to substitute the fossil fuel in near future. Biomass is also available in almost every part of the world. Fortunately, Malaysia is rich in its agricultural residue such as palm oil solid waste, coconut shell, rice husk and many more. Theses waste can be utilized as an alternate energy source rather than to be dumped. As a matter of fact, land disposal is causing serious environmental pollution to the environment. Among the various biomass wastes available in Malaysia, oil palm solid waste has tremendous potential to be utilized as a fuel to generate a combustible producer gas. In this study, co-combustion of diesel oil and producer gas, from a downdraft gasifier, was done in an experimental combustion chamber. The combustion behaviour and emissions properties of the co-combustion process were analyzed. Experimentation was done for combustion of diesel oil alone as well as combustion of producer gas alone and co-combustion of liquid fuel and producer gas. Data were recorded at different equivalence ratio and producer gas flows. It was found that that the producer gas can be co-combusted with liquid fuel. The emission data shows that the co-combustion process produces more CO, NO_x, SO_2 and CO_2 compared to the combustion of diesel oil only. However, the exhaust temperature for the co-combustion process is considerable higher than the diesel combustion only which can utilized in obtaining higher boiler pressures and temperatures.

Key words: biomass, co-combustion, emissions, oil palm solid waste, producer gas.

1. INTRODUCTION

World energy consumption is increasing every year due to increased population. The rising quality of life and industrialization has also contributed to the demand for energy resources. It is estimated that current world population is 6.4 billion people living on earth today and half of it is below 25 years old. So it is expected that the world population will rise in near future so will be the demand in energy (Donald 2000).

In Malaysia, the main energy resource is petroleum. It contributes to about 68 % of total consumption and mainly used for transportation, industry, power generation

* Faculty of Mechanical Engineering, Universiti Teknologi Malaysia, 81310, Skudai, Johor, Malaysia
Email: ahmad@siswa.utm.my
** Department of Energy & Environment Engineering, QUEST, Nawabshah, Pakistan.
Email: srsamo@yahoo.com
*** Faculty of Mechanical Engineering, Universiti Teknologi Malaysia, 81310, Skudai, Johor, Malaysia
Email: ahmad@siswa.utm.my

etc. However, these natural resources are decreasing every year because it high consumption. Nevertheless, fossil fuel utilization also creates environment concerns..

Combustion of fossil fuel such as coal and petrol produce harmful gases like carbon monoxide (CO) and sulfur dioxide (SO_2). Even the cleanest fossil fuels produce carbon dioxide when it burns. Carbon dioxide is a harmless gas but build up of this gas in the atmosphere may cause greenhouse effect (Nicholas 1981).

Understandably there is a need to find another source of energy to curb the oil consumption to the minimum possible level and to increase the utilization efficiency and also to minimize the pollution from energy generation. An alternative energy that can be practice in Malaysia is energy from biomass. Some of common biomass resources that available in Malaysia are woods, agricultural residue and crops.

Most of these biomass energy resources such as agricultural residue are left abandon without being used for other purpose. Palm oil solid waste is one of the most potential biomass resources which can be used as an energy source. The first commercial oil palm estate in Malaysia was set up in 1917. Since then the industry in Malaysia has grown by leaps and bounds and the country is now the largest producer and exporter of palm oil with 67.6 million tonnes of fresh fruit bunch is received by palm oil mill in 2003. Palm oil is expected to demonstrate an annual growth of 4.57% every year. In January 2005 her production of palm oil is about 13.97 millions tons and the total soild wastes generated by this industry has amounted to more than 3.6 millions tons (PORIM 2005). Production is expected to reach 26.2 million tonnes by the year 2005, and anticipated to account for around 20% of the global oils and fats supply.

With this condition, it is estimated that every one million tonnes of palm oil produces 0.8 million tonnes of palm oil shell. With this large amount of palm oil shell solid waste, there is a need to find several ways to utilize this waste. Recently, there is several usage of palm oil shell waste. It is used as a fuel for boiler in the palm oil mill (Razuki 1988).

Biomass gasification is one of the chemical processes to convert biomass solid residue into usable fuel such a producer gas. Producer gas is generated when the biomass is burned with less air to achieve complete combustion. Producer gas is mainly contained carbon monoxide (CO), hydrogen (H_2), methane (CH_4), water vapour, and some other inert gases. Mixed with air, producer gas can be used in the internal combustion engine with a little modification (Donald et. al., 1981). Also it can be used as a co-combustion fuel with other liquid fuel to minimize the fuel consumptions. Producer gas from the gasification process can be utilized in many ways. Fig. 1 show the various ways of utilizing producer gas and the variable involve.

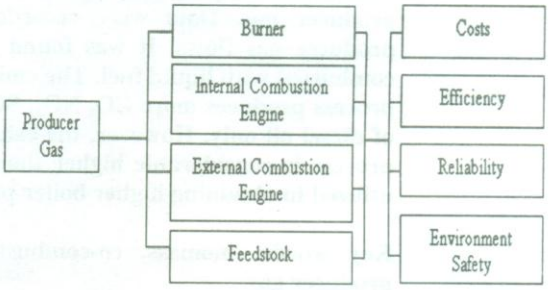

Figure 1.Various ways of producer gas utilization

Gasification offers the cleanest, most efficient method available to produce synthesis gas from low or negative-value carbon-based feed stocks such as coal, petroleum coke, high sulphur fuel oil or materials that would otherwise be disposed as waste. Gasification adds value to low- or negative-value feed stocks by converting them to marketable fuels and products. Gasification technologies differ in many aspects but share certain general production characteristics. Different types of fixed bed gasifiers are shown in Fig. 2.

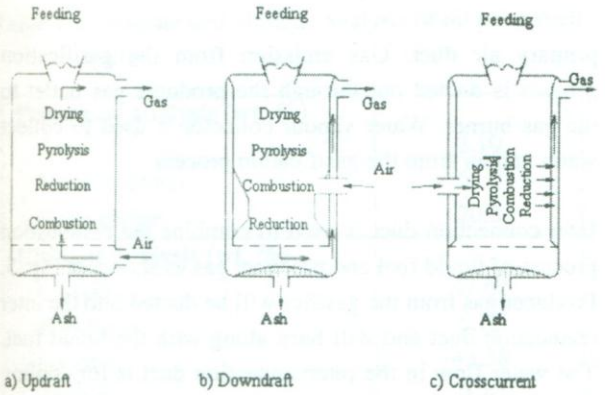

Figure 2. Types of fixed bed gasifiers

The high temperature in the gasifier converts the inorganic materials in the feedstock (such as ash and metals) into a vitrified material resembling coarse sand. Fixed bed gasification is an important commercial gasification process. A recent survey of gasifier manufacturers were found that 75% of the gasifiers were downdraft, 20% were fluid beds and only 2.51% were updraft and 2.5% were other types.

For this study, a downdraft gasifier is used to produce the producer gas. In the downdraft gasifier the tar have to pass through the hot combustion and reduction zones. A schematic diagram of the downdraft gasifier is shown in Fig. 3.

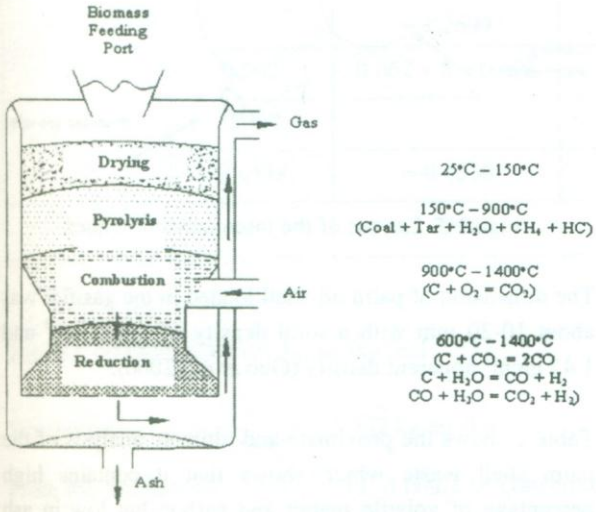

Figure 3. Downdraft gasifier used for experimentation

If the gasifier is properly designed, it will lead to sufficient combustion and cracking of the tar to make the gas useful with minimal cleaning process.

2. CO-COMBUSTION OF BIOMASS

Co-combustion of biomass is to burn biomass fuel with other type of fuel simultaneously. The fuel can be any type of fuel such as fossil fuel. Recently, there have been several designs that use producer gas as fuel for co-combustion. This concept has been applied to the internal combustion engine and burner. It sometimes called dual fuel engine or dual fuel burner.

Gasification process generally uses reactants such as oxygen or steam to increase gas yields while consuming char. In systems where solid fuels are gasified in the presence of sub stoichiometric air, several chemical reactions occur. Gasification reaction and temperature zone are shown in Fig. 3.

In this case, there is a surplus of solid fuel, carbon dioxide and water vapor from the combustible zone can be passed through the glowing layer of charcoal and are reduced to carbon monoxide (CO) and hydrogen (H_2) in the region known as the reduction zone (Naksite 1989).

In the combustion zone, the reactions which are exothermic are:

$$C+O_2 \rightarrow CO_2 \quad \rightarrow (1)$$

$$2H_2+O_2 \rightarrow 2H_2O \quad \rightarrow (2)$$

The reaction in the reduction zone which are endothermic, will decrease the temperature during the reduction process are :

$$C + CO_2 \rightarrow 2CO \quad \rightarrow (3)$$

$$C + H_20 \rightarrow CO + H_2 \quad \rightarrow (4)$$

$$C + 2H_2 \rightarrow CH_4 \quad \rightarrow (5)$$

$$CO + 3H_2O \rightarrow CH_4 + H_2O \quad \rightarrow (6)$$

$$C + 2H_2O \rightarrow CO_2 + H_2 \quad \rightarrow (7)$$

$$CO + H_2O \rightarrow CO_2 + H_2 \quad \rightarrow (8)$$

Producer gas is therefore a mixture of the gaseous such as hydrogen (H_2), carbon monoxide (CO), carbon dioxide (CO_2), nitrogen (N_2), methane (CH_4), and small amount of other hydrocarbons. The combustible components of the gas are CO, H_2, CH_4 and C_xH_x, the percentages of which should be made as high as possible. The quantity of CO in the gas depends on the temperature in the reduction zone. To achieve complete reduction, the temperature in the reduction zone must be at least 1100°C (Henry 1981).

If water vapor is present, reaction (4) play an important role to enrich the gas with H_2 and thus enhance its heating value. However, if too much water is present, CO may react with H_2O to form CO_2 and H_2, as indicated by reaction (8) and the quantity of CO may be reduced.

3. MATERIALS AND METHOD

For this experiment, downdraft gasifier is used for the gasification process. Fig. 4 shows the picture of the experimental setup and it component.

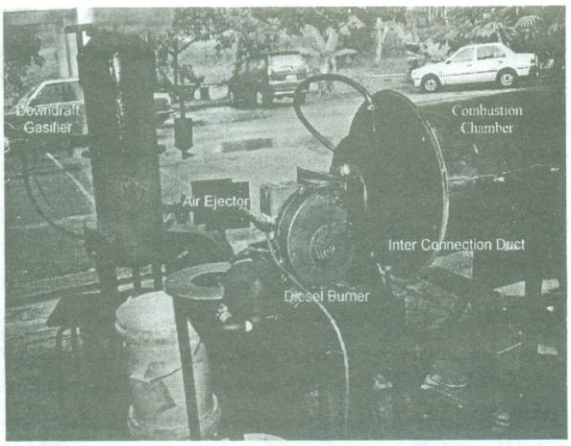

Figure 4. Picture of the experimental setup

The setup consisted of downdraft gasifier, air ejector, Inter connection duct, oil burner, gas analyzer and air blower. A small quantity of air is needed for combustion process, and the air is blown using a blower through the primary air duct. Gas emission from the gasification process is ducted out through the producer gas outlet to the gas burner. Water vapour collector is used to collect water vapour from the gasification process.

Inter connection duct is used to combine the combustion process of liquid fuel and producer gas as shown in Fig. 5. Producer gas from the gasifier will be ducted into the inter connection duct and will burn along with the liquid fuel. The water flow in the interconnection duct is for cooling the interconnection duct during the experiment. This is to prevent any hazard during the experiment because without coolant it will become very hot and it is really dangerous. It is also used as an energy converter to burn the producer gas.

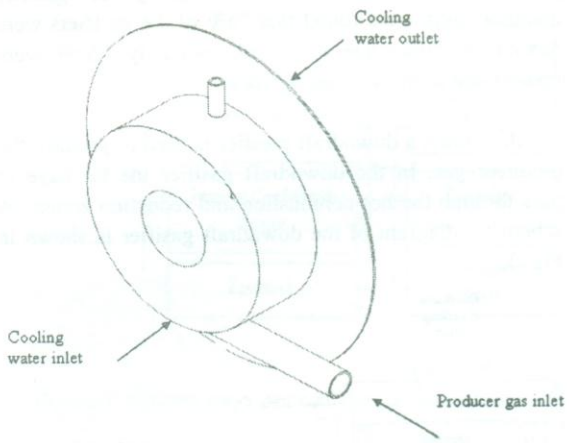

Figure 5. Layout of the interconnection duct

The dimension of palm oil shell loaded in the gasifier was about 10-20 mm with a solid density of 1.53 g/cm^3 and 1.47 g/cm^3 apparent density (Guo *et al.*, 2000).

Table 1 shows the proximate and ultimate analysis of the palm shell waste which shows that it contains high percentage of volatile matter and carbon but low in ash (Ani 1992).

Table 1. Proximate and ultimate analysis of oil palm shell waste

Proximate analysis (wt. %)	
Ash	2.10
Volatile matter	67.0
Fixed carbon	20.3
Ultimate analysis (wt. %)	
Carbon	47.62
Hydrogen	6.20
Oxygen	43.38
Nitrogen	0.70
Moisture (wt. % air dry)	9.70
Low Calorific Value (MJ/kg)	19.10

Using the ultimate analysis of the palm shell waste, calculations were done for the stoichiometic air requirement for the gasifier. The sample calculation procedure is outlined in Table 2.

required is less than stoichiometric i.e. less than 50% required.

The experimental work comprised of three distinct experiments. These were done to compare and analyse the emission properties of combustion with different fuel condition and properties. The experiments were as follows:

i) Combustion of diesel oil

ii) Combustion of producer gas

iii) Co-combustion of diesel oil and producer gas

The mass flow rate of the diesel oil used in the burner was 0.001195 kg/s.

Table 2. Stoichiometric air requirement using oil palm shell waste as fuel

Constituent	Mass constituent kg/kg fuel	O_2 required kg/kg fuel	Product of combustion kg/kg fuel		
			CO_2	H_2O	N_2
C	0.4762	$0.4762 \times 2\frac{2}{3} = 1.2699$	$0.4762 \times 3\frac{2}{3} = 1.7461$		0.4762 x 8.84 = 4.21
H_2	0.062	0.062 x 8 = 0.496		0.062 x 9 = 0.558	0.062x 26.5 = 1.643
N_2	0.007				= 0.007
O_2	0.4338	=-0.4338			-0.4338 x 0.768 = -0.3332
Total		1.3321	1.7461	0.558	5.5268

Total O_2 required = 1.3321 kg air /kg fuel

Stoichiometric air = $\frac{1.3321}{0.232}$ = 5.742 kg air /kg fuel

From the stoichiometric mass of air, it could be converted to volume flow rate and for gasification the amount of air

Combustion of diesel fuel

The diesel fuel burner was used for this experiment. Before starting the experiment, the cooling water circulation is regulated to assist the cooling process in the combustion chamber and in the interconnection duct. The

combustion chamber is preheated using the diesel burner for fifteen minute to prevent heat losses during the experiment.

The diesel burner was set with different baffle air opening to get a different equivalent ratio setting. Data was recorded for equivalence ratio (Φ) ranging from 0.9-1.2. The emission data was analyzed using the TELEGAN gas analyzer.

Combustion of producer gas

After the experiment of diesel fuel combustion was completed, the diesel fuel burner was turn off to allow the combustion of producer gas to proceed. Before the experiment, producer gas was needed to be generated using the downdraft gasifier. Before starting the experiment, all connection in the gasifier was checked to prevent any gas leakage. Gasifier is start up by filling the bottom of the bed with charcoal to assist for reduction process to generate producer gas. Then, the gasifier is filling up with palm oil shell until 1/2 of the gasifier bed. Then it was ignited by adding a little petrol. After it is ignited, it is left for 15 minute until it was fully ignited. Primary air supply valve is open to full and the windowpane is left opened (Lukeman 2004).

After that, the feeding process is continued by filling the gasifier with palm oil shell until it is full to about three quarter. Then the windowpane is closed and properly tightens. The primary air valve is reduced to 1/4 valve opening. This is to generate the producer gas because producer gas is generated when solids burn with less air supply. Secondary air valve is opened to 1/4 valve opening. After a few minute one can see white thick smoke flow to the interconnection duct and then to the combustion chamber. The producer gas is then ignited using burning paper through the burner port in the interconnection duct.

The burning process if left for a few minute to wait it to become stable before data is recorded. After the burning process is stable, data is recorded for 1/4 and 1/2 secondary valve opening.

Co-combustion of diesel oil and producer gas

After the experiment on combustion of producer gas, the experiment is proceeded to the co-combustion of diesel oil and producer gas experiment. Before starting the experiment, the gasifier must feed with palm oil shell. It is because during the experiment of producer gas, it is burned and turn into ash. This will reduce the amount of palm oil shell in the gasifier and also reduce the producer gas generation. After that, the feeding process is continued by filling the gasifier with palm oil shell until 3/4 full.

The windowpane is closed, and diesel burner is turn on. It is left for a few minute before data is recorded. Data is recorded for 1/4 and 1/2 secondary air valve opening and equivalent ratio (Φ) equal to 0.9, 1.0 (stoichiometric), 1.1 and 1.2. Graph for value of gas emission, combustion temperature versus equivalent ratio is plotted.

4. RESULT AND DISCUSSION

Equivalence ratio (Φ) is used to indicate quantitatively whether a fuel oxidizer mixture is fuel rich, lean or stoichiometric. For $\Phi>1$ the mixture is fuel rich, $\Phi<1$ the fuel is fuel lean, and $\Phi=1$ the fuel mixture is stoichiometric (Stephen 2000). The emissions were plotted as a function of equivalence ratio for diesel combustion only as shown in Fig. 6. Also O_2 and CO_2 graph were also plotted as function of equivalence ratio. It was found that by increasing the equivalence ratio, the NO_x, SO_2 and CO_2 formation was increased during the diesel combustion process. Fig. 7 shows that the O_2 percentage decreased with the increase of equivalent ratio. Fig. 8, shows that with the increase in equivalence ratio the exhaust temperature also increased. At stoichiometric condition the exhaust temperature was 680 °C.

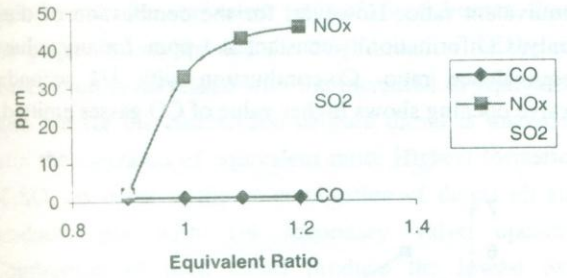

Figure 6. Emissions profile for diesel combustion

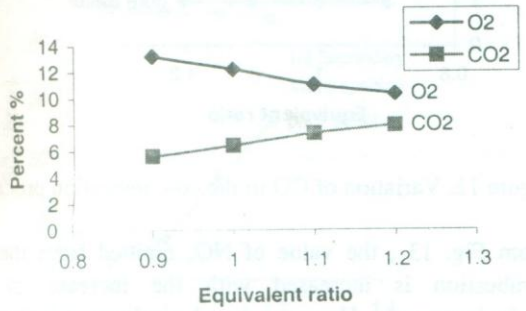

Figure 7. Variation of O_2 and CO_2 for diesel combustion

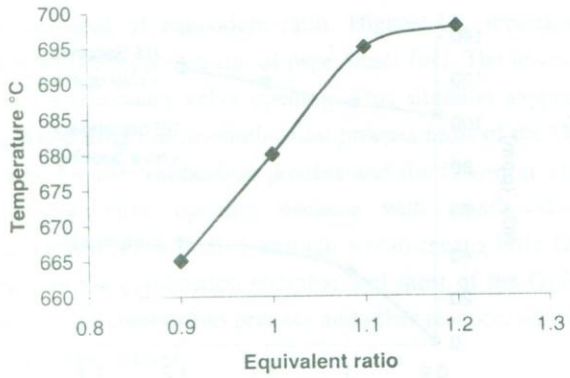

Figure 8. Temperature profile for the diesel combustion

For the combustion experiment for producer gas combustion only, the data was collected based on two secondary air valve opening, 1/4 and 1/2. The secondary air valve is used to control the amount of producer gas flow to the interconnection duct for burn in the combustion chamber and also as an air supply for the combustion of producer gas.

The formation of CO, NO_x and SO_2 increased with bigger valve opening as shown in Fig. 9. For O_2 and CO_2 it shows a very little reduction with the increase of valve opening as reported in Fig. 10. Compared with CO and SO_2, NO_x shows the highest production with 1/4 valve opening but it shows the lowest with 1/2 valve opening. This situation may cause of with bigger valve opening, more air and producer gas is ducted to the combustion chamber and this mean that more producer gas is burn and produces more CO, SO_2 and NO_x.

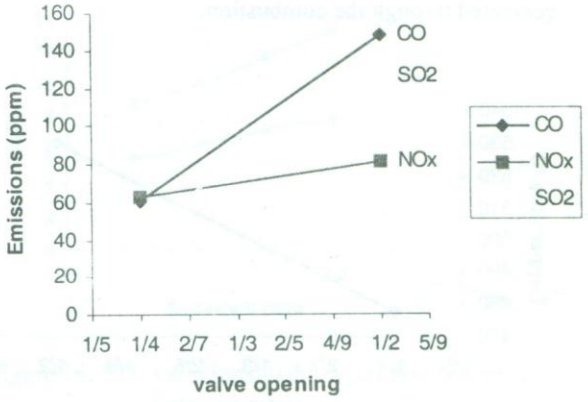

Figure 9. Emissions profile for the combustion of producer gas from downdraft gasifier

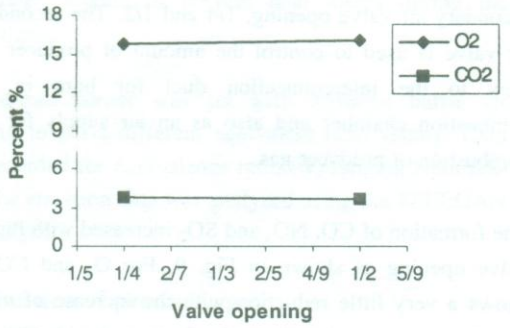

Figure 10 . Variation of O_2 and CO_2 for the producer gas combustion

From Fig. 11 it can be seen that the combustion temperature is increased with the increased of secondary valve opening. It is because with bigger valve opening more air is ducted through and also more producer gas flow to the combustion chamber and more heat are generated through the combustion.

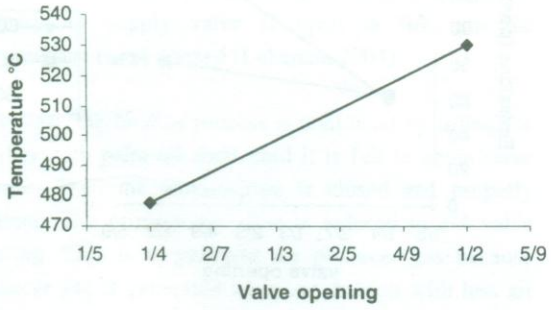

Figure 11. Temperature (°C) profile for the combustion of producer gas

Co-combustion of diesel and producer gas was done for different secondary valve opening and equivalent ratio of diesel fuel burner. Emission data has been plotted and is compared with of the combustion of diesel. Fig. 12 shows that the value of CO is decreased with the increase of equivalent ratio. However, for the combustion of diesel only, CO formation is constant at 1 ppm for any value of equivalence ratio. Co-combustion with 1/4 secondary valve opening shows higher value of CO gasses emitted.

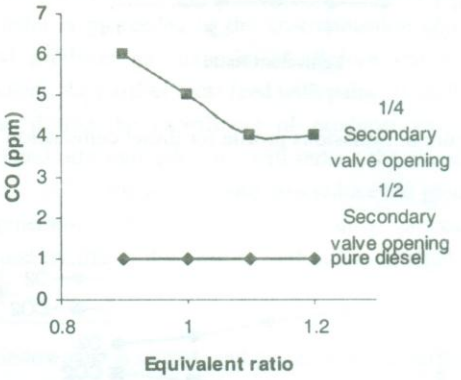

Figure 12. Variation of CO in the co-combustion process

From Fig. 13 , the value of NO_x emitted from the co-combustion is increased with the increase of the equivalence ratio. However diesel combustion it shows a rapid increase from the equivalent ratio of 0.9 to the stoichiometric condition. When $\Phi>1$ NO_x emission show a little increase. Co-combustion with 1/4 secondary valve opening shows the highest of NO_x emission of and the lowest is pure diesel combustion.

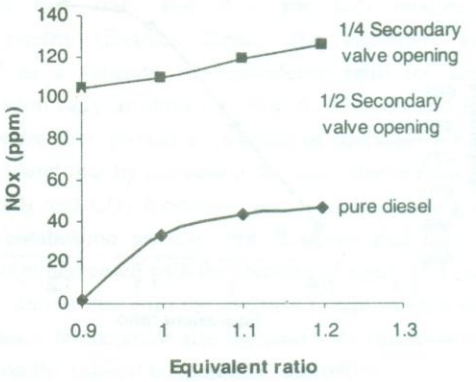

Figure 13. NOx emission behaviour in the co-combustion process.

Fig. 14 show the graph for the emission value of SO_2 (ppm) versus the equivalent ratio of diesel burner. From the graph we can see that the SO_2 formation for the co-combustion is decreased with the increased of equivalent ratio but for the combustion of pure diesel is increased with the increased of equivalent ratio. Highest formation of SO_2 is occur at the co-combustion of diesel oil and producer gas with 1/4 secondary valve opening. Combustion of pure diesel produce the lowest SO_2 emission compared to the combustion of the fuel combination.

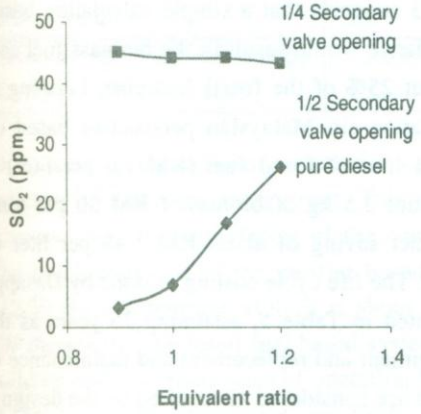

Figure 14. Variation of SO_2 in the co-combustion process

From Fig.15, the value of O_2 emission (%) decreased with the increased of equivalent ratio. Highest O_2 emission occur with the combustion of pure diesel fuel. The lowest is at 1/4 secondary valve opening. This situation happen because during the co-combustion process most of the O_2 is used for the combustion process and the lowest at 1/4 secondary valve opening because with small valve opening less air is ducted through which means little O_2 flow into the combustion chamber and most of the O_2 is used for the combustion process and other reaction which formed other gasses.

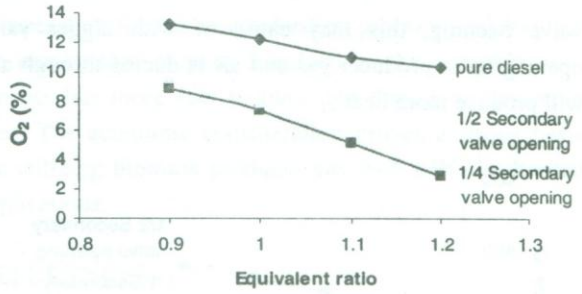

Figure 15. Variation of O_2 in the co-combustion process

According to Fig. 16, it shows that the amount of CO_2 emitted is increased with the increased of equivalent ratio value. Equivalent ratio $\Phi>1$ means that the fuel burn with less air which cause incomplete combustion. Incomplete combustion will produce more CO_2. The highest CO_2 emission is at 1/4 secondary valve opening and the lowest is during the combustion of pure diesel.

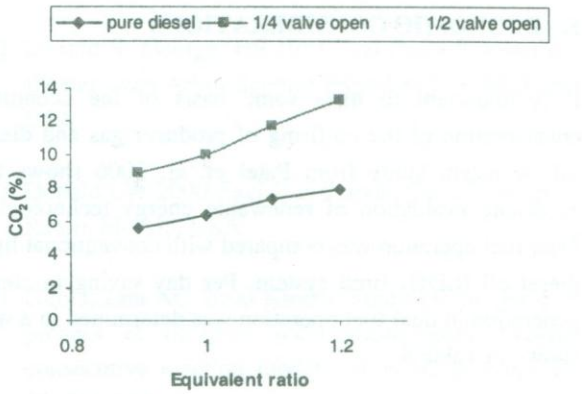

Figure 16. CO_2 variations in the co-combustion process

Fig.17 show the graph of combustion temperature for pure diesel combustion and the fuel combination versus the equivalent ratio. From the graph it shows that the temperature is increased with the increased of equivalent ratio. Temperature from the co-combustion with producer gas is higher compared to the temperature for pure diesel fuel combustion. Highest temperature is 1/2 secondary

valve opening, this may cause of with bigger valve opening more producer gas and air is ducted through and will produce more heat.

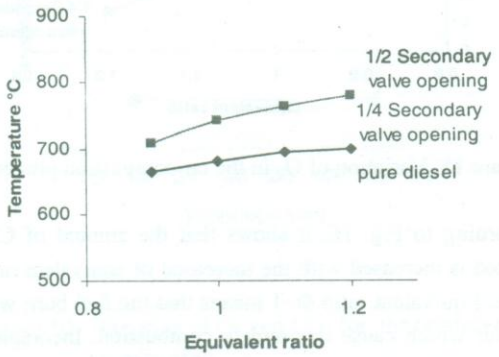

Figure 17. Temperature (°C) profile for the co-combustion process

5. ECONOMIC CONSIDERATIONS

It is important to have some basis of the economic consideration of the co-firing of producer gas and diesel oil. A recent study from Patel et. al. 2006 shows the economic evaluation of renewable energy technologies. Dual fuel operation was compared with conventional light diesel oil (LDO) fired system. Per day saving in steam generation in dual fuel operation was determined in a way shown in Table 4.

Economic analysis of the gasifier system showed that user could save about RM 31.40 per hour (about 39 % cost saving) by using dual fuel (60% LDO + 40% producer gas) for steam generation. This proves the economic economic viability of the gasifier-based operation. The pay back period for the gasifier system can be around 1000 h of operation or using the system for about 67 days (15 hr/day operation).

A similar study from Dasappa et al., 2003 shows that about 3 kg of biomass replaces about 1 liter of diesel. Patel et al 2003 suggests that a simple calculation based on the mass balance would result in the biomass fuel cost amount to about 25% of the fossil fuel cost. Looking at the said calculation sin Malaysian perspective based on the fuel cost, 1 liter of fossil fuel (RM 1.6 per liter) is replaced by about 3.5 kg of biomass (RM 30 per ton); resulting in a net saving of about RM 1.49 per liter of diesel replaced. The life cycle costing as done by Dasappa (ibid) is presented in Table 5, assuming 25 years as the life of the equipment and replacement and maintenance of the components are considered as required by the design.

Table 4. Comparison of fuel cost: net LDO and dual fuel mode operation (adopted from Patel *et al.* 2006)

Fuel used	LDO consumption liter/hr	Biomass consumption Kg/hr	Total cost of fuel per hr (RM)	Saving (RM./hr)	Saving per day (15 hr of operation per day) RM
LDO (100%)	50	-	80	-	-
LDO(60%) + producer gas (40%)	30	78.8	48.8	31.4	471

Cost of LDO = RM 1.6 per liter, Cost of palm shell waste = RM 30/ton, 1 US $ = 3.70 Ringgit

Table 5. Economic of the gasifier based operation for thermal applications (adopted from Dasappa *et al.* 2003).

Life cycle cost estimates	Gasifier based systems	Diesel based systems
Initial capital cost (RM per kW thermal)	445.31	37.50
Life cycle O&M cost (RM per kW thermal)	141.82	56.73
Life cycle fuel cost (RM per kW thermal)	709.16	4538.50
Total life cycle cost (RM per kW thermal)	1296.3	4648.12
Overall unit cost of energy (cents per kW thermal)	3.63	12.82

In presenting the economic analysis, various costs are indicated as the input energy cost. This approach would eliminate the efficiency factor of the conversion device. The investment cost of the gasifier based system is RM 412.50 per kW thermal while it is about RM 37.50 per kW thermal for the fossil fuel based system including the building cost, the economics of operation are as presented in Table 4. The economics are fairly attractive even without the CO_2 cost benefits. The entire investment is realized in about 2 years. This proves a strong basis for utilizing biomass producer gas with LDO in thermal applications.

6. CONCLUSION

The producer gas generated from the downdraft gasifier can be used as an alternative fuel for combustion.. It can be used for power generation such as gas turbine, gas burner, heating process etc. Experimental results shows that co-combustion of diesel oil and producer gas emitted more CO, NOx, SO_2, and CO_2. For CO, NOx, SO_2, and CO_2 gasses, the highest gas emitted is with 1/4 secondary valve opening. Combustion of pure diesel oil has the highest level of O_2 gasses compared to the combustion of fuel combination. The lowest O_2 emitted is with co-combustion with 1/4 secondary valve opening. Temperature for the co-combustion process is higher than the combustion of pure diesel oil as the co-combustion process has more fuel to burn and thus generates more heat. The economic consideration proves a strong basis for utilizing biomass producer gas with LDO in thermal applications.

REFERENCES

[1] Ani F N 1992 Thermal characteristics of oil palm fruit shells. In: *Proceedings of the second international energy conference- Energy from biomass residues*, Kuala Lumpur, Malaysia, November 3-5, 1994.

[2] Dasappa, S., Sridhar, H.V., Sridhar, G., Paul, P.J. and Mukunda, H.S. (2003) Biomass gasification - a substitute to fossil fuel for heat application. *Biomass and Bioenergy* 25: 637-649.

[3] Donald K, George HE 1981 Fuel *From Biomass and Wastes*, Ann Arbor Science Publisher Inc., Michigan, USA.

[4] Donald LW 2000 *Fuel Gas System*, ORC Press, Boca Raton, Florida, USA.

[5] Guo J, Lua AC 2000 Kinetic Study on the pyrolytic process of oil-palm solid waste using two-step consecutive reaction model. *Biomass & Bioenergy* 20, 223-233.

[6] Henry KB 1981 *Energy the Biomass Option*, John Wiley and Son Inc, New York, USA.

[7] Lukeman Y 2004 Pressurized induced flow on downdraft gasifier system with low emission burner, MS thesis, Faculty of Mechanical Engineering, Universiti Teknologi Malaysia, Johor, Malaysia.

[8] Naksite C 1989 *Biomass Gasification Research and Field Development*, Prince of Songkhla University, Thailand.

[9] Nicholas P C 1980 *Biomass Application, Technology and Production*, Marcell Dekker Inc, New York, USA.

[10] Patel, S.R., Bhoi, P.R. and Sharma, A.M. (2006) Field-testing of SPRERI's open core gasifier for thermal application. *Biomass and Bioenergy* 30: 580–583.

[11] PORIM 2005 *A summary of the performance of the Malaysian Oil Palm Industry – A weekly update.* Palm Oil Research Institute of Malaysia, Kualalumpur, Malaysia, (http://www.mpob.gov.my).

[12] Razuki I 1988 Gasification of Biomass, MS Thesis, Faculty of Mechanical Engineering, Universiti Teknologi Malaysia, Johor, Malaysia.

[13] Stephen RT 2000 *An Introduction To Combustion Process*, McGraw Hill, Singapore.

EFFECT OF MICROSTRUCTURAL CONSTITUENTS ON ABRASIVE WEAR RESISTANCE OF CARBURIZED SAE 8822H STEEL

Muhammad Hayat Jokhio*, Muhammed Ibrahim Panhwar** and Mujeeb-u-ddin Memon***

ABSTRACT

The main object of the present work is to investigate the effect of various microstructural constituents on the abrasive wear resistance of carburized SAE 8822H steel. For this purpose the specimens were carburized and heat-treated at various parameters, so as to obtain different microstructural phases. Metallographic investigations were carried out using optical microscope, electron microscope, and x-ray diffractometer. The abrasive wear resistances were recorded in weight loss in grams method, using 120-mesh emery paper fixed on rotating disc of the wear-testing machine. The experimental results shows that the abrasive wear resistance of carburized SAE 8822H depends upon the presence of various microstructural constituents as discussed in results.

1. INTRODUCTION

SAE 8822H steel is used for manufacturing tractor's transmission parts, which under goes complex-loading conditions where the fatigue and abrasive wear is also involved. Therefore the present work is an initial attempt to investigate the effect of microstructural constituents on abrasive wear resistance of carburized SAE 8822H steel.

The main object of carburizing is to enhance the fatigue durability and wear resistance of machine parts made from various carburizing steels. Carburizing heat treatment results to produce high hardened fracture resistance case lying over a soft but tougher core [1-2]. For high fatigue and wear properties required in case and core structures in carburized parts are usually under goes various heat treatments followed by quenching and tempering [3]. As the carburizing process alter the chemical composition of case and core, therefore, the proper heat treatment after carburizing is also an essential parameters for controlling the microstructure in case and core for high fatigue and wear resistance [4]. The fatigue and wear damage in carburized case is essentially starts at the surface. Therefore improvements in fatigue and wear properties in case structure are still a research-oriented topic. Most of the previous work consists on fatigue resistance of carburized components [1-4, 6-9 and 11]. However vary little information is available on wear resistance of carburized parts. Abrasive wear damage is involved in most of the rotating machine parts, when a hard particle slide or roll under pressure across a surface or in contacting subsurface of parts [5,10]. Some of previous work was done to investigate the effect of various treatments on microstructure and fatigue resistance of carburized parts made from carburizing steel [3,5,6 and 11].

2. EXPERIMENTAL PROCEDURE

2.1 MATERIAL AND SPECIMEN PREPARATION

SAE 8822H steel which contained 0.25%C, 0.24%Si, 0.78%Mn, 0.012%P, 0.039%S, 0.37%Ni, 0.46%Cr, and 0.36%Mo by weight in hot forged condition in the form

* Associate Professor, Department of Metallurgy and Materials Engineering, MUET, Jamshoro.
** Professor, Department of Mechanical Engineering, MUET, Jamshoro.
*** Professor, Department of Mechanical Engineering, MUET, Jamshoro.

of pinion has been used in experimental work. The forged material was isothermally annealed at 925°C for 60 minutes and slowly cooled through the transformation range to refine the grain size and to improve Machinability. Specimens of 20 mm diameter and 40 mm length were machined from annealed material.

2.2 HEAT TREATMENT

All specimens were gas carburized to 925°C in continuous carburizing furnace using endothermic atmosphere enriched in propane. The carbon potential during carburizing and diffusion was maintained at 0.15-0.17 and 0.28-0.3 vol% Co respectively. The specimens were air cooled after carburizing for further reaustenitizing treatments. The specimens were grouped into 5 lots and each lot was given various heat treatments. The detail of this is given in Table 1.

Table 1: Various Heat Treatment Specimen

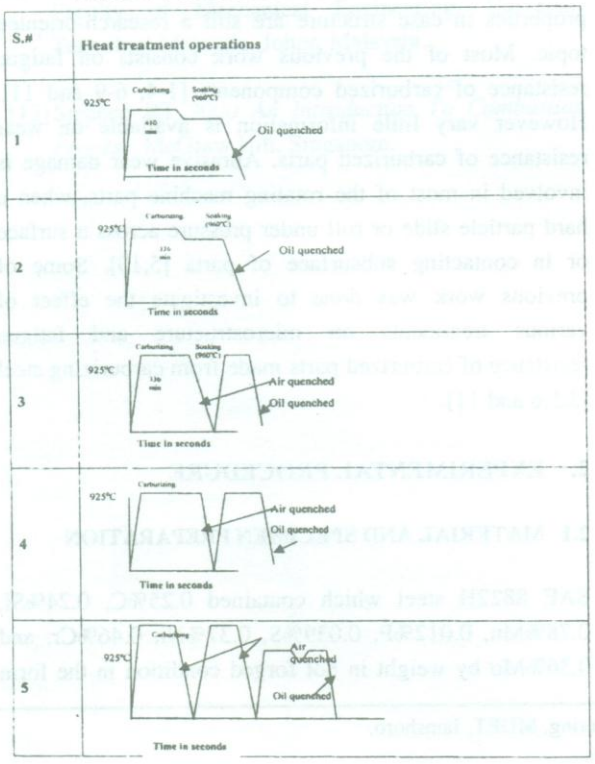

2.3 MEASUREMENT OF SURFACE CARBON AND CASE DEPTH

The surface carbon and carbon gradient was measured from the test bar by machining at 0.2 mm interval. The chips were collected for the carbon analysis by carbon combustion method. The surface carbon content of specimens was found to be 1.1 to 0.8 weight percent. The effective case depths were also determined using Vickers hardness tester and measured 513 VHN from surface to words the core of all specimens using 500 grams load. The detail of this investigation is given in tables 2,3 and 4.

Table 2: Measurement of Carbon Concentration Gradient

Sp No:	C from surface to core in mm	0.00	0.20	0.40	0.60	0.80	1.0	1.20	1.40	1.40
1		1.1 %	1.1 %	.92 %	.77 %	0.65 %	0.60 %	0.55 %	0.46 %	0.40 %
2		0.85 %	0.80 %	0.75 %	0.63 %	0.55 %	0.50 %	0.44 %	0.40 %	0.38 %
3,4,5		1.00 %	0.94 %	0.85 %	0.70 %	0.60 %	0.55 %	0.52 %	0.45 %	0.40 %

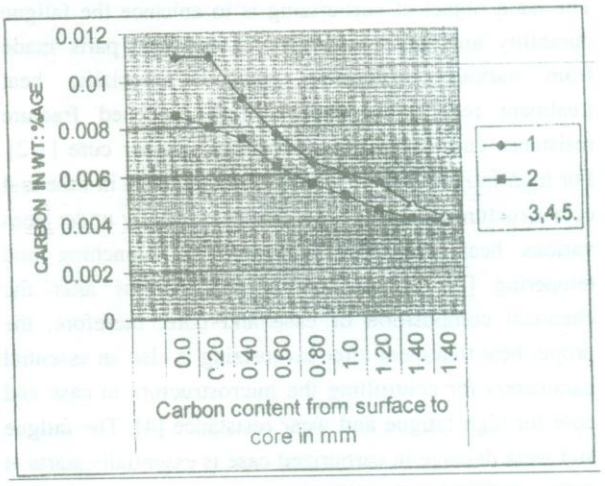

Fig. 1: Measurement of Carbon Concentration Gradient

Table 3: Measurement of Hardness

Specimen No.	Hardness' Before Heat Treatment	Surface Hardness	Core Hardness
1	161.35	772	455
2	161.35	805	441
3	161.35	726	434
4	161.35	772	441
5	161.35	778	434

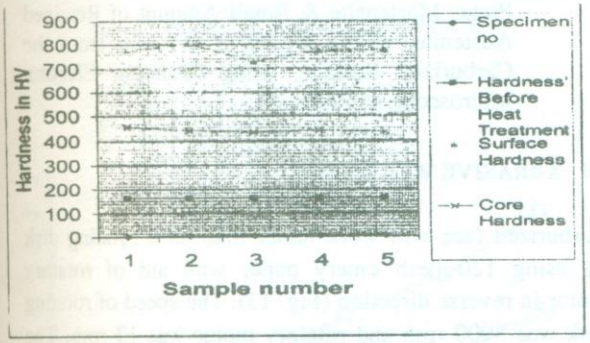

Fig. 2: Measurement of Hardness

Table 4: Measurement of Case Depth

Specimen No.	Effective Case Depth	Total Case Depth
1	1.50	1.80
2	1.10	1.60
3	1.60	1.60
4	1.60	1.60
5	1.60	1.60

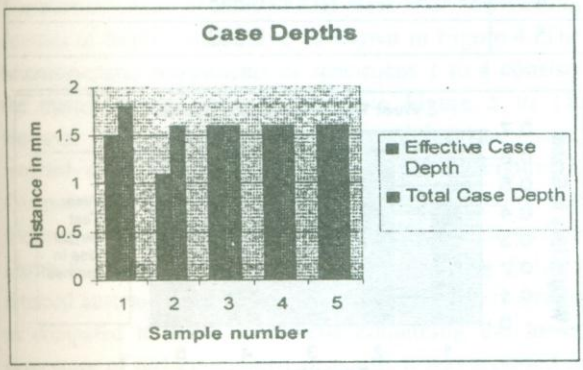

Fig. 3: Measurement of Case Depth

2.4 METELLOGRAPHY AND DETERMINATION OF MICROSTRUCTURAL CONSTITUENTS

Microstructural constituents were investigated by using optical microscope, and scanning electron microscope. The quantities of retained austenite and martensite were also investigated by using standard x-ray diffraction techniques. The area under the diffraction peaks (200) for martensite and (220) for retained austenite was measured as recommended by Phillips and George, et al [7and 8]. The results of this investigation are shown in Figure 4 to 11.

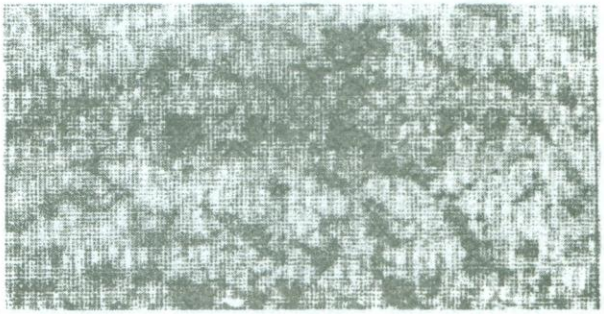

Fig. 4: Shows Ferrite Pearlite Microstructure of SAE 8822H Steel Before Heat Treatment 2000X

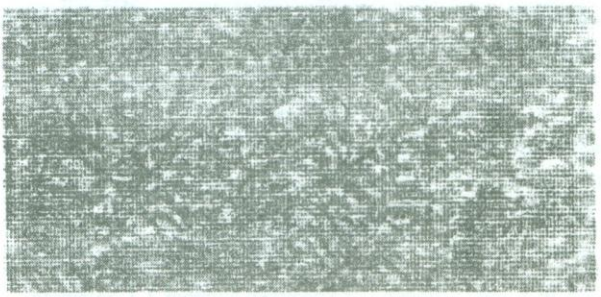

Fig. 5: Shows 30% Retained Austenite White and Martensite using Optical Microscopes 2000x

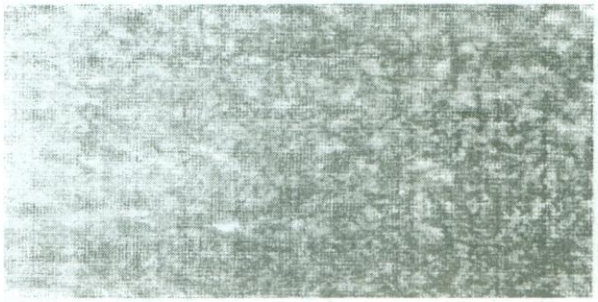

Fig. 6: Shows 25% Retained Austenite Martensite using Optical Microscopes 2000x

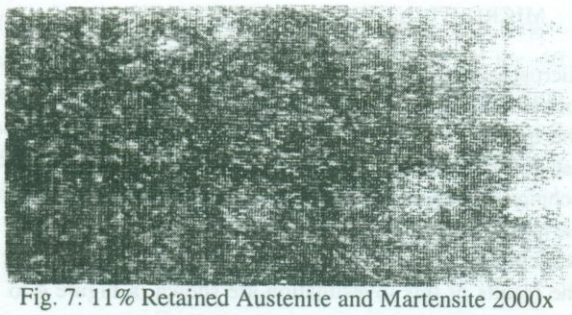

Fig. 7: 11% Retained Austenite and Martensite 2000x

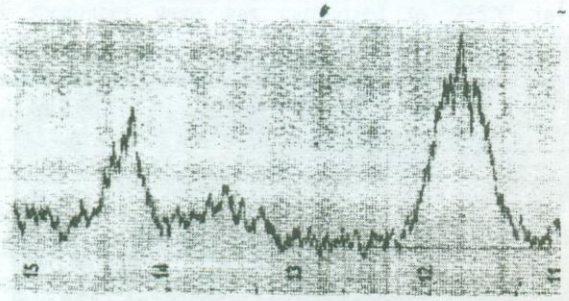

Fig. 8: X-ray Diffraction of Specimen Number 1, Containing (200) Peaks of Martensite & (220) Peaks of Retained Austenite, using X-Ray Diffractometer

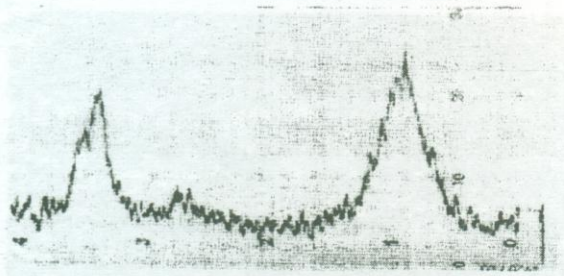

Fig. 9: X-ray Diffraction of Specimen Number 2, Containing (200) Peaks of Martensite & (220) Peaks of Retained Austenite, using X-Ray Diffractometer.

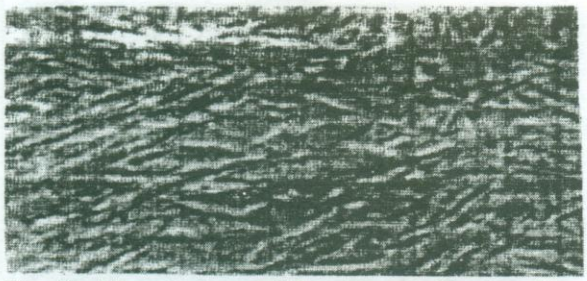

Fig. 10: Microstructure of Specimen 2, Showing Plate Martensite & Retained Austenite, at the Depth of 0.1mm from the Carburized Surface, using Scanning Electron Microscopes at 5000x

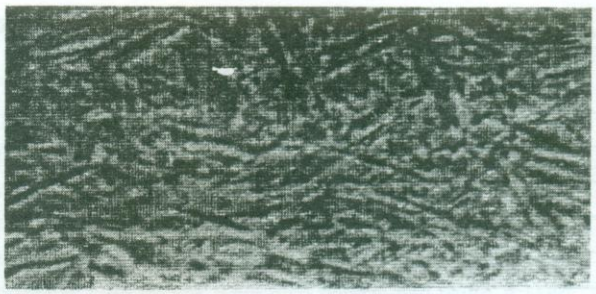

Fig. 11: Microstructure of Specimen 4, Showing Large Plates Martensite & Small Amount of Retained Austenite, at the Depth of 0.1 mm from the Carburized Surface, using Scanning Electron Microscope at 5000x.

2.5 ABRASIVE WEAR TEST

Carburized face was worn under load on a rotating disk by using 120-mesh emery paper with aid of rotatory motor in reverse direction (Fig. 13). The speed of rotating disk was 3000 rpm and rotatory motor was 12 rpm. The weight applied was 2680 grams. Each lot was worn at same parameters. The emery paper was changed after each hour period of testing and the weight loss in grams of each lot was recorded on electron balance. The abrasive wear test results of each lot vs time are shown in Figure 14.

Table 5: Measurement of Abrasive Wear

S. No.	Wear Test Weight Loss in Gram
1	0.455
2	0.639
3	0.639
4	0.645
5	0.302

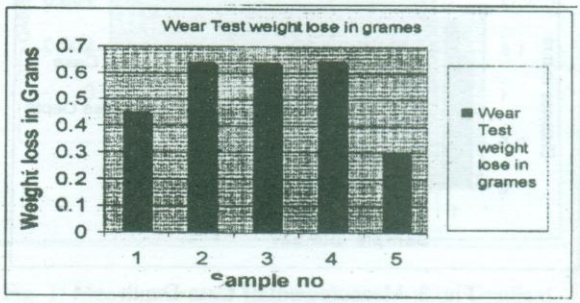

Fig. 12: Measurement of Abrasive Wear Resistance

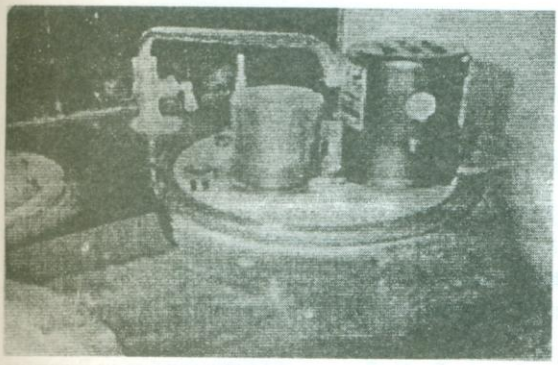

Fig. 13: Abrasive Wear Testing Machine

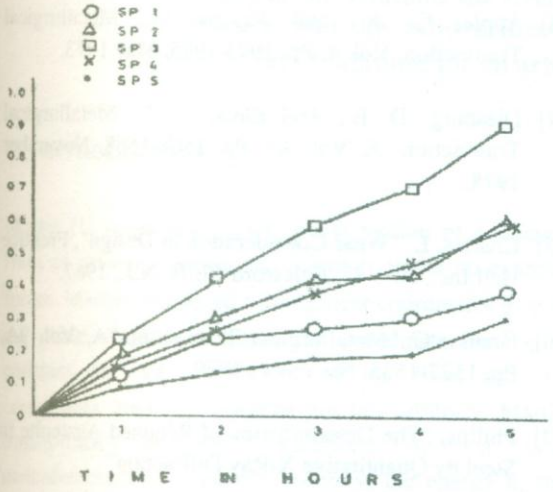

Fig 14: Abrasive Wear Resistances of Steel Samples

3. RESULTS AND DISCUSSIONS

The microstructure of SAE 8822H steel after normalizing consists of ferrite and pearlite as shown in Figure 4. The Microstructural constituents of specimens 1 to 4 consists the martensite and retained austenite Figure 5 to 11. However the specimen number 5 containing martensite, retained austenite and carbide is shown in Figure 7. Comparison of the abrasive wear profile among the specimens which contains the retained austenite at surface shows that the specimen number 1 containing heights retained austenite (30%) has lowest weight loss in grams as compared to those specimens containing the lower percentage of surface retained austenite. It was reported in early literature that retained austenite is soft which would decrease the abrasive wear resistance and must be avoided in carburized components, later on it was conventionally wisdom that it must be present in the carburized components. The increasing amount of retained austenite would decrease the fatigue and wear resistance of the carburized cases [1 and 5]. Fournella, R. A., et al investigating the effect of retained austenite on fatigue resistance of carburized components observed that increasing the amount of retained austenite in the carburized cases does not decrease the fatigue resistance. They have also observed that under cyclic loading condition retained austenite work hardened and transforms into martensite provided the additional mode for surface comprehensive stress, which would result to increase the fatigue strength of carburized case. Jason J. Spice and David K. Matlock investigate the effectiveness of three different techniques, designed to improve the bending fatigue life in comparison to conventionally processed gas-carburized 8620 steel. The bending fatigue samples were machined from forged gear blanks from the same lot of material used for the pinion gear tests, and all processing of laboratory samples and gears was done together. Fatigue data were obtained on standard as carburized parts and after three special processing histories: shot peening to increase surface residual stresses; double heat treating to refined austenite grain size. He has observed that shot peening also proved to be the most effective way to improve fatigue life at both imposed torque levels. The results of this study show that data on laboratory samples can be used to interpret the fatigue performance of gears.

The highest weight loss in grams was found in the specimen containing lowest weight percent of retained austenite (11%), as the same was reported by Apple, C.A., and Krauss, G[3& 6]. They were of the opinion that martensite contains larger number of submicro cracks which decreases the fatigue strength of carburized case. In case of specimen number 5 which shows the fine martensite, retained austenite and spherical fine carbides has the lowest weight loss as compared to all other specimens and resulted the over all highest abrasive wear resistance [11]. The same effect was observed by number of investigators [3, 9, and 10]. Apple and Krauss have observed that a double reaustenitizing treatment has provided fine martensite, which increased the fatigue strength of carburized case. Siepak, J has observed that

high-retained austenite is beneficial for contact wear resistance. Jokhio, et al has investigated the effect of reaustenitizing treatment on abrasive wear resistance of carburized steel and found that double reaustenitizing treatment produced fine martensite with retained austenite that does not decreased the abrasive wear resistance of carburized steel.

4. CONCLUSIONS

1. The abrasive wear resistance of carburized SAE 8822H steel does not decrease with increasing carbon the amount of retained austenite up to 30% by volume.
2. Retained austenite network hardened and transformed to martensite thus increased the wear resistance and provided additional compressive stress.
3. The abrasive wear resistance of carburized components does not increased with increasing hardness value but increased with quantity of retained austenite. It shows that abrasive wear resistance rather depends on amount of retained austenite and some other factors like fines of martensite plates, spherical carbides, and carbon content in the martensite and retained austenite.
4. The surface carbon content (1.1 weight percent, alloy content Ni, Cr, Mo), austenitizing conditions (quenching from 860 °c to 140 °c in oil after carburizing) and double reaustenitizing had refined the case structure and increased the abrasive wear resistance.
5. The double reaustenitizing treatment is recommended for the production of carburized components where the high abrasive wear resistance is to be considered as the designing factor.

ACKNOWLEDGMENTS

The authors are highly indebted to Professor Dr. Mutfa Durk, Head of the Department of Metallurgy and Materials Science, Middle East Technical University, for his continuous support, and cooperation during the experimental work carried out at Middle East Technical University and HEMA Gear Factory, Ankra, Turkey. The authors extend there thanks to the authorities Mehran University of Engineering & Technology Jamshoro, Sindh, Pakistan for providing the facilities of reaustenitizing.

REFERENCES

[1] Parish, G., And Harper, G. S., "Production of Carburising" Pigment Press, p 1-289, 1985

[2] Parish, G., "Influence of Microstructure on Properties of Case Carburized Components" ASM, Ohio, 1980.

[3] Apple, C. A., and Krauss, G., Metallurgical Transaction, Vol. 4, Pp. 1973 1995, May 1973.

[4] Diesburg, D. E., And Eldis, G. T., Metallurgical Transaction- A, Vol. 9A, Pp. 1561-1568, November 1978.

[5] Charles, L. "Wear Consideration in Design", Prentice Hall Inc., 00.1 47, Egleword Cliffs, N.J., 1967.

[6] Krauss, G., Metallurgical Transaction- A, Vol. 9A, Pp. 1527-1535, November 1979.

[7] Philips, "The Determination of Retained Austenite in Steel by Quantitative X-Ray Diffraction"

[8] George, T. El. D., Journal of Heat Treating, Volume 1, No.3, Pp 24-30, 980. Siepak, J., Wear, 80, Pp. 301-205, 1982.

[9] Fournella, R. A., Et Al, Journal of Heat Treating, Volume 2, No.1, Pp 54-61, ASM,1981.

[10] Jokhio, M. H., Et Al, Quarterly, Mehran University Research Journal of Engineering & Technology, Volume 15, No.1, Jamshoro, January 1995.

[11] Jason J. Spice and David K. Matlock Optimized Carburized Steel Fatigue Performance Colorado School of Mines Society of Automotive Engineers, Inc. 2002.

SOME STEADY PLANE FLOWS OF AN INCOMPRESSIBLE NEWTONIAN FLUID

Rana Khalid Naeem*, Waseem Ahmed Khan** and Roohi Bano**

ABSTRACT

The equations describing the steady plane motion of an incompressible Newtonian fluid neglecting viscous dissipation for an arbitrary state equation are transformed into Martin's system (ϕ, ψ) in which the coordinate lines ψ = constant are the streamlines of the flow and the coordinate lines ϕ = constant are left arbitrary. Some exact integrals of the transformed equations are determined for radial, vortex and parallel flows. In some of the solutions the stream function ψ or the viscosity μ or both are arbitrary, and this arbitrariness indicates that the flow equations have an infinite set of solutions for an arbitrary state equation.

1. INTRODUCTION

Martin [1] considered steady plane motion of a viscous fluid of constant density and viscosity under no external forces. Martin introduced a curvilinear coordinates ϕ, ψ in the plane of flow in which the coordinate lines ψ = constant are the streamlines of the flow and the coordinates lines ϕ = constant are left arbitrary. Martin transformed the flow equations into a new underdetermined system for vorticity, the energy h, the pressure p and the coefficients E, F, G of the first fundamental form $ds^2 = E\,d\phi^2 + 2F\,d\phi\,d\psi + G\,d\psi^2$ as functions of ϕ, ψ. Martin studied some flows by placing certain conditions a priory on the coefficients E, F, G and determined exact solutions for these flows. Nath [2] extended Martins approach to the plane flows of compressible fluids. Nath showed that when the streamlines ψ = constant of the steady, plane flow of a compressible fluid are taken as one set of the coordinate lines in a curvilinear coordinate system ϕ, ψ in the physical plane, the equations governing the flow can be replaced by a new system of equations. Nath proved that for steady, plane flows of compressible fluids (i) the only flows of prim fluids with straight streamlines are either simple source flows or straight parallel flows (ii) if the energy is constant along each streamline then the flow fields are either the general vortex flows or flows in parallel straight lines (iii) when the velocity magnitude is constant along each streamline, the flow fields are the general vortex flows or flows in parallel straight lines. Naeem [3] generalized Martins method to the viscous compressible Navier-Stokes equations. Naeem dealt with viscous compressible non-adiabatic gases which have a multiplicity of flows for a given streamline pattern, and obtained various solution sets for a prescribed flow pattern. Naeem [4], employing one-parameter group of transformations, determined some exact solutions of the equations governing the motion of an incompressible fluid of variable viscosity. Naeem [5] has recently conducted mathematical study of the Navier-Stokes equations for incompressible fluid of variable viscosity using Hodograph method, and determined some exact solutions.

Pinarbasi and Liakopoulos [6] have studied stability of plane poiseuille flow for liquids exhibiting exponential

* Department of Mathematics & Basic Sciences, NED University of Engineering & Technology, Karachi.

** Department of Mathematics, University of Karachi, Karachi.

viscosity temperature dependence. Their study indicated that the primary flow is affected through the variation of viscosity with temperature. The critical Reynolds number decreases considerably compared to isothermal poiseuille flow and the influence of Prandtl number, temperature fluctuations, viscosity fluctuations on the flow stability are small. In the present work, we reconsider their continuity, momentum balance and energy balance equations with the objective of obtaining exact integrals for radial, vortex and parallel flows for an arbitrary state equation.

2. GOVERNING EQUATIONS

We consider two dimensional steady flow of an incompressible, Newtonian fluid. The continuity, momentum balance and energy balance equations (neglecting viscous dissipation) can be written as [6]:

$$\frac{\partial \bar{u}_i}{\partial x_i} = 0 \qquad \rightarrow (1)$$

$$\bar{\rho} u_i \frac{\partial \bar{u}_j}{\partial x_i} = -\frac{\partial \bar{p}}{\partial x_j} + \frac{\partial \bar{\tau}_{ij}}{\partial x_i}, j = 1,2 \qquad \rightarrow (2)$$

$$\bar{u}_i \frac{\partial \bar{T}}{\partial x_i} = \frac{\bar{K}}{\bar{\rho} C_p} \frac{\partial}{\partial x_i}\left(\frac{\partial \bar{T}}{\partial x_i}\right) \qquad \rightarrow (3)$$

Where the summation convention is used over index i. In the equations above, $\bar{\rho}$ denotes fluid density, $\bar{K}$ is the thermal conductivity, $\bar{C}_p$ is the specific heat constant at constant pressure, $\bar{\rho}$ is the pressure, $\bar{u}_i$ is the i th component of the velocity vector, $\bar{\tau}_{ij}$ is the (i, j) – th component of the deviatoric stress tensor and $\bar{T}$ denotes the temperature. For Newtonian incompressible fluid

$$\bar{\tau}_{ij} = \bar{\mu}\left(\frac{\partial \bar{u}_i}{\partial x_j} + \frac{\partial \bar{u}_j}{\partial x_j}\right) \qquad \rightarrow (4)$$

Introducing dimensionless variables based on the reference velocity $\bar{U}$, viscosity μ_o, temperature T_o, characteristic length $\bar{L}$, i.e.,

$$x_i = \frac{\bar{x}_i}{\bar{L}}, u_i = \frac{\bar{u}_i}{\bar{U}}, p = \frac{\bar{p}}{\bar{\rho}\bar{U}^2}, \mu = \frac{\bar{\mu}}{\bar{\mu}_o}, T = \frac{\bar{T}}{\bar{T}_o} \qquad \rightarrow (5)$$

The flow governing equations are transformed to,

$$\frac{\partial u_i}{\partial x_i} = 0 \qquad \rightarrow (6)$$

$$u_i \frac{\partial u_j}{\partial x_i} = -\frac{\partial p}{\partial x_j} + \frac{1}{Re}\frac{\partial \tau_{ij}}{\partial x_i}, j = 1,2 \qquad \rightarrow (7)$$

$$u_i \frac{\partial T}{\partial x_i} = \frac{1}{Re\,Pr}\frac{\partial}{\partial x_i}\left(\frac{\partial T}{\partial x_i}\right) \qquad \rightarrow (8)$$

In equation (7)

$$\tau_{ij} = \mu\left(\frac{\partial u_i}{\partial x_j} + \frac{\partial u_j}{\partial x_i}\right) \qquad \rightarrow (9)$$

and the Reynolds and Prandtl numbers are defined as

$$Re = \frac{\bar{\rho}\bar{U}\bar{L}}{\bar{\mu}_o} \quad \text{and} \quad Pr = \frac{\bar{\mu}_o \bar{C}_p}{\bar{k}}$$

The equation of continuity (6) implies the existence of a stream functions $\psi = \psi(x, y)$ such that

$$u = \frac{\partial \psi}{\partial y}, v = -\frac{\partial \psi}{\partial x} \qquad \rightarrow (10)$$

We take $\phi(x, y)$ = constant to be some arbitrary family of curves which generates with the streamlines $\psi(x, y)$ = constant a curvilinear net, so that in the physical plane the independent variables x, y can be replaced by ϕ, ψ.

Let

$$x = x(\phi, \psi), y = y(\phi, \psi) \qquad \rightarrow (11)$$

define a curvilinear net in the (x, y) – plane with the squared element of arc length along any curve given by

$$ds^2 = E(\phi, \psi)d\phi^2 + 2F(\phi, \psi)\, d\phi\, d\psi + G(\phi, \psi)d\psi^2 \quad \rightarrow (12)$$

where

$$E = \left(\frac{\partial x}{\partial \phi}\right)^2 + \left(\frac{\partial y}{\partial \phi}\right)^2$$

$$F = \frac{\partial x}{\partial \phi}\frac{\partial x}{\partial \psi} + \frac{\partial y}{\partial \phi}\frac{\partial y}{\partial \psi}$$

$$G = \left(\frac{\partial x}{\partial \psi}\right)^2 + \left(\frac{\partial y}{\partial \psi}\right)^2 \quad \rightarrow (13)$$

Equations (11) can be solved to obtain $\phi = \phi(x, y)$, $\psi = \psi(x, y)$ such that

$$\frac{\partial x}{\partial \phi} = J\frac{\partial \psi}{\partial y}, \frac{\partial x}{\partial \psi} = -J\frac{\partial \phi}{\partial y}$$

$$\frac{\partial y}{\partial \phi} = -J\frac{\partial \psi}{\partial x}, \frac{\partial y}{\partial \psi} = J\frac{\partial \phi}{\partial x} \quad \rightarrow (14)$$

provided $0 < |J| < \infty$, where J is the transformation Jacobian and,

$$J = \frac{\partial x}{\partial \phi}\frac{\partial y}{\partial \psi} - \frac{\partial x}{\partial \psi}\frac{\partial y}{\partial \phi} = \pm\sqrt{EG - F^2} = \pm W \quad \rightarrow (15)$$

Following Martin [1] and Naeem [3], we transform equations (6 – 9) into the ϕ, ψ - coordinates and we have the following theorem:

Theorem 1:

If the streamlines ψ (x, y) = constant of an incompressible fluid of variable viscosity is chosen as one set of coordinate curves in a curvilinear coordinate system ϕ, ψ in the physical, then the equations (6 – 9) in the (x, y) – coordinates may be replaced by the system:

$$J\omega = -JH_\psi + R\phi\left\{\frac{(J^2 - F^2)\cos 2\alpha}{E} + \frac{2FJ\sin 2\alpha}{E}\right\}$$

$$+ R_\psi\{F\cos 2\alpha - J\sin 2\alpha\}$$

$$+ Q_\phi\left\{\frac{FJ\cos 2\alpha}{E} + \frac{(F^2 - J^2)\sin 2\alpha}{2E}\right\}$$

$$- Q_\psi\{J\cos^2\alpha + F\sin\alpha\sin\alpha\} \quad \rightarrow (16)$$

$$JH_\phi = R_\phi\{J\sin 2\alpha - F\cos 2\alpha\} + R_\psi E\cos 2\alpha$$

$$+ Q_\phi\{F\sin\alpha\cos\alpha - J\sin^2\alpha\} - Q_\psi E\sin\alpha\cos\alpha \quad \rightarrow (17)$$

$$\omega = \frac{1}{W}\left[\left(\frac{F}{W}\right)_\phi - \left(\frac{E}{W}\right)_\psi\right] \quad \rightarrow (18)$$

$$\left[\left(\frac{GT_\phi - FT_\psi}{J}\right)_\phi + \left(\frac{ET_\psi - FT_\phi}{J}\right)_\psi\right] = \mathrm{Re}\,\mathrm{Pr}T_\phi \quad \rightarrow (19)$$

$$\left[\left(\frac{W}{E}\Gamma_{11}^2\right)_\psi \left(\frac{W}{E}\Gamma_{12}^2\right)_\phi\right] = 0 \quad \rightarrow (20)$$

of five equations for seven functions E, F, G, H, T, μ and ω of ϕ, ψ. In equations (16 – 20)

$$R = \frac{\mu}{JRe\sqrt{E}}[q_\phi(J\sin 2\alpha - F\cos 2\alpha + q\alpha_\phi(F\sin 2\alpha + J\cos 2\alpha)$$

$$+ q_\psi E\cos 2\alpha - qE\sin 2\alpha\alpha_\psi] \quad \rightarrow (21)$$

$$Q = \frac{4\mu}{JRe\sqrt{E}}[(F\sin\alpha + J\cos\alpha)(q_\phi\cos\alpha - q\alpha_\phi\sin\alpha)$$

$$- E\,\mathrm{Sin}\alpha\left(q_\psi\mathrm{Cos}\alpha - q\alpha_\psi\mathrm{Sin}\alpha\right) \quad \rightarrow (22)$$

$$q = \frac{\sqrt{E}}{W} \quad \rightarrow (23)$$

$$H = p + \frac{1}{2}\frac{E}{W^2} - \frac{2\mu}{Re}\frac{(F\sin\alpha + J\cos\alpha c}{J\sqrt{E}}(q_\phi \cos\alpha - q\sin\alpha\alpha_\phi)$$

$$-\frac{\sqrt{E}\sin\alpha}{J}(q_\psi \cos\alpha - q\sin\alpha s_\psi)] \quad \rightarrow(24)$$

$$\Gamma_{11}^2 = \frac{1}{2W^2}\left[-F\frac{\partial E}{\partial\phi} + 2E\frac{\partial F}{\partial\phi} - E\frac{\partial E}{\partial\psi}\right] \quad \rightarrow(25)$$

$$\Gamma_{12}^2 = \frac{1}{2W^2}\left[E\frac{\partial G}{\partial\phi} - F\frac{\partial E}{\partial\psi}\right] \quad \rightarrow(26)$$

The system of equations (16 – 20) is underdetermined since it involves two more unknown functions than number of equations. This is due to the arbitrariness of the coordinate curves ϕ = (x, y) = constant and the state equation. We can reduce the unknown functions by one by choosing the (ϕ, ψ) – system to be orthogonal and in this case F = 0.

In the present work we determine the solutions of the equations (16 – 20) by placing a prior condition on the matrices E, F, G. To achieve our objective we introduce an orthogonal system (ξ, η) such that η = constant represents streamlines. In (ξ, η) – net, the first fundamental element is given by

$$ds^2 = g_1^2 d\xi^2 + g_2^2 d\eta^2 \quad \rightarrow(27)$$

Where g_1 (ξ, η) and g_2 (ξ, η) are the matrices of the net. Choosing the (ϕ, ψ) – net to be orthogonal, we get F = 0. Employing F = 0, $\phi = \phi(\xi)$ and $\psi = \psi(\eta)$ in equation (12), we get

$$ds^2 = E\phi'^2 d\xi^2 + G\psi'^2 d\eta^2 \quad \rightarrow(28)$$

The equations (27) and (28), on comparison, give

$$E = \frac{g_1^2}{\phi'^2}, G = \frac{g_2^2}{\psi'^2}, W = \frac{g_1 g_2}{\phi'\psi'} \quad \rightarrow(29)$$

Employing F = 0, $\psi = \psi(\eta)$, $\phi = \phi(\xi)$ and the equations in the theorem 1 can be transformed to the (ξ, η) – net, yielding the following theorem:

Theorem 2:

If a natural (ξ, η) coordinate system is selected, where η = constant are streamlines and ξ = constant are the orthogonal trajectories, the equations governing the flow of an incompressible fluid of variable viscosity in theorem 1 takes the form:

$$\omega = -\frac{H_\eta}{\psi'} + g_2 R_\xi \frac{\cos 2\alpha}{g_1\psi'} - R_\eta \frac{\sin 2\alpha}{\psi'}$$

$$-g_2 Q_\xi \frac{\sin 2\alpha}{2g_1\psi'} - Q_\eta \frac{\cos 2\alpha}{\psi'} \quad \rightarrow(30)$$

$$H_\xi = R_\xi \sin 2\alpha + g_1 R_\eta \frac{\cos 2\alpha}{g_2} - g_1 Q_\eta \frac{\sin\alpha\cos\alpha}{g_2}$$

$$-Q_\xi \sin^2\alpha \quad \rightarrow(31)$$

$$\omega = -\frac{1}{g_1 g_2}\left(\frac{g_1\psi'}{g_2}\right)_\eta \quad \rightarrow(32)$$

$$\left(\frac{g_2 T_\xi}{g_1}\right)_\xi + \left(\frac{g_1 T_\eta}{g_2}\right)_\eta = Re\,Pr\,\psi' T_\xi \quad \rightarrow(33)$$

$$\left(\frac{g_{2\xi}}{g_1}\right)_\xi + \left(\frac{g_{1\eta}}{g_2}\right)_\eta = 0 \quad \rightarrow(34)$$

Where

$$R = \frac{\mu}{Re}\left[\frac{-\psi'(-g_{2\xi}\,2\sin 2\alpha + g_{1\eta}\cos 2\alpha)}{g_1 g_2^2} + \left(\frac{\psi'^2}{g_2^2}\right)_\eta \frac{\cos 2\alpha}{2\psi'}\right] \rightarrow(35)$$

$$Q = \frac{4\mu}{Re}\left[\frac{\psi'(-g_{2\xi}\cos 2\alpha + g_{1\eta}\sin\alpha\cos\alpha)}{g_1 g_2^2} - \left(\frac{\psi'^2}{g_2^2}\right)\frac{\sin\alpha\cos\alpha}{2\psi'}\right] \rightarrow(36)$$

$$H = p + \frac{1}{2}\frac{\psi'^2}{g_2^2} - \frac{2\mu}{Re g_1}\left(q_\xi \cos^2\alpha - q\alpha_\xi \sin\alpha\cos\alpha\right) + \frac{\left(q\alpha_\eta \sin\alpha - q_\eta \cos\alpha\right)}{g_2} \quad \rightarrow(37)$$

$$q = \frac{\psi'}{g_2} \quad \rightarrow(38)$$

3. SOLUTIONS

In this section we seek the solutions of the equations in theorem 2 for various prescribed flow geometries.

3.1 CIRCULAR FLOW

For circular flow

$$\eta = r, \xi = \theta, g_1 = r, g_2 = 1, \alpha = -\theta \quad \rightarrow(39)$$

Substituting equations (39) in equations (30 – 38), we get

$$H_r = \frac{\psi'}{r}(r\psi')_r + \frac{B_\theta}{r} - B_r \sin 2\theta \quad \rightarrow(40)$$

$$H_\theta = -B_\theta \sin 2\theta + rB_r + 4B\sin^2\theta \quad \rightarrow(41)$$

$$r^2T_{rr} + rT_r + T_{\theta\theta} - r\,Re\,Pr\,\psi' T_\theta = 0 \quad \rightarrow(42)$$

Where

$$B = \frac{\mu}{Re}\left(\psi''(r) - \frac{\psi'(r)}{r}\right) \quad \rightarrow(43)$$

The equations (40 – 42) constitute a system in four unknown functions H, ψ, μ and T. We require one more equations to make this system determinate. The equation is determined by employing the compatibility condition $H_{r\theta} = H_{\theta r}$. This condition provides an equation that must be satisfied by the functions ψ and μ. This equation is

$$r^2B_{rr} + 3rB_r - B_{\theta\theta} = 0 \quad \rightarrow(44)$$

Equation (44) possesses solutions for the following cases:

Case I: $B = 0$

Case II: $B \neq 0$

We consider these two cases separately.

Case I:

When B = 0, equation (44) is identically satisfied and equation (43) yields:

$$\psi = c_1\frac{r^2}{2} + c_2 \quad \rightarrow(45)$$

Where $c_1 (\neq 0)$ and c_2 are arbitrary constants. We note that in this case the viscosity μ is arbitrary.

Equation (42), utilizing equation (45), becomes:

$$r^2T_{rr} + rT_r + T_{\theta\theta} - c_1r^2\,Re\,Pr\,T_\theta = 0 \quad \rightarrow(46)$$

The coefficients in equation (46) suggests to seek a solution of the form

$$T = c_3\theta + c_4M(r) \quad \rightarrow(47)$$

and the solution is

$$T = c_3\theta + (c_5 + c_6\ln r) + \frac{c_3c_1r^2}{4c_4}Re\,Pr \quad \rightarrow(48)$$

Where c_3, $c_4 (\neq 0)$, c_5 and $c_6 (\neq 0)$ are arbitrary constants. Equations (40) and (41), on utilizing B = 0 and equation (45), yield

$$H = c_1^2r^2 + h_1 \quad \rightarrow(49)$$

Where h_1 is an arbitrary constant.

Case II:

When $B \neq 0$, we require to solve equations (42) and (44). The solution of equation (42) depends on the form of the coefficient of the term T_θ. A solution of equation (42) exists when

$$r\,Re\,Pr\,\psi' = Constant = \lambda(say) \quad \rightarrow(50)$$

Which gives

$$\psi = \frac{\lambda}{\mathrm{Re\,Pr}} \ln r + c_9 \qquad \rightarrow (51)$$

The solution of equation (44) is

$$B = c_7 r^{-1+\sqrt{2}} + c_8 r^{-1-\sqrt{2}} \qquad \rightarrow (52)$$

Where c_7 ($\neq 0$), c_8 ($\neq 0$), and c_9 are arbitrary constants. The equation (42), using equation (50), becomes

$$r^2 T_{rr} + r T_r + T_{\theta\theta} - \lambda T_\theta = 0 \qquad \rightarrow (53)$$

This equation has two solutions, and these are

$$T = \begin{cases} Y(r) e^{c_{10}\theta} \\ c_{15}\theta + A(r) \end{cases} \qquad \rightarrow (54)$$

Where

$$Y(r) = \begin{cases} c_{11} r^{\sqrt{\lambda c_{10} - c_{10}^2}} + c_{12} e^{-\sqrt{\lambda c_{10} - c_{10}^2}} & , \lambda - c_{10} > 0 \\ c_{13} \cos(m \ln r) + c_{14} \sin(m \ln r) & , \lambda c_{10} - c_{10}^2 < 0 \\ & \lambda c_{10} - c_{10}^2 = -m^2, m > 0 \end{cases} \qquad \rightarrow (55)$$

and

$$A(r) = (c_{16} + c_{18} \ln r) + \frac{\lambda}{2} c_{15} r^2 \qquad \rightarrow (56)$$

In equations (54 – 56) c_i (i=10,..,18) are all non-zero constants. The viscosity μ, in this case, is given by

$$\mu = -\frac{\mathrm{Re}^2 \mathrm{Pr}}{2\lambda} \left(c_7 r^{1+\sqrt{2}} + c_8 r^{1-\sqrt{2}} \right) \qquad \rightarrow (57)$$

Since viscosity μ is always non-negative, the constant $\lambda<0$ or the constants are simultaneously negative valued. In this case the function H is given by

$$H = \theta(rB_r + 2B) - B \sin\theta + c_9 \qquad \rightarrow (58)$$

Where B is given by equation (52)

3.2 RADIAL FLOW

For this type of flow

$$\eta = \theta, \xi = r, g_1 = 1, g_2 = r, \alpha = \theta \qquad \rightarrow (59)$$

Using equation (59) in equations (30 – 38), we obtain

$$\frac{H_\theta}{\psi'} - \frac{\psi''}{r^2} = \frac{r\psi''}{\psi'} B_r + \frac{B_\theta}{\psi'} \left[4\psi' \cos^2\theta + \psi'' \sin 2\theta \right]$$

$$+ \frac{B}{\psi'} \left[8\psi'' \cos^2\theta - 4\psi' \sin 2\theta + \psi''' \sin 2\theta \right] \qquad \rightarrow (60)$$

$$H_r = B_r \left[-4\psi' \sin^2\theta + \psi'' \sin 2\theta \right] + \frac{B_\theta}{r} \psi''$$

$$+ \frac{B}{r} \left[-4\psi' + \psi''' \right] \qquad \rightarrow (61)$$

$$r^2 T_{rr} + r T_r - r\,\mathrm{Re\,Pr}\,\psi'(\theta) T_r + T_{\theta\theta} = 0 \qquad \rightarrow (62)$$

Where

$$B = \frac{\mu}{\mathrm{Re}\, r^2} \qquad \rightarrow (63)$$

Employing integrability condition $H_{r\theta} = H_{\theta r}$ and equation (63), we obtain

$$2\mu\psi^{IV} + 2\mu'\psi''' + 4\mu'\psi' + \mu''\psi'' + 4\mu\psi'' = -2\,\mathrm{Re}\,\psi'\psi'' \qquad \rightarrow (64)$$

Treating equation (64) a differential equation in μ, we obtain

$$\mu = \frac{\int \left(\frac{b_1 - \mathrm{Re}\,\psi'^2}{\psi''} \right) M(\theta) d\theta + b_2}{M(\theta)} \qquad \rightarrow (65)$$

Where

$$M(\theta) = \exp\left\{ \int \left(\frac{\psi''' + 4\psi'}{\psi''} \right) d\theta \right\} \qquad \rightarrow (66)$$

and b_1, b_2 are arbitrary constants. We note that in equations (65) and (66), the function ψ is arbitrary at this

stage. We now determine the solutions of the equation (62) which also provide the function ψ. The equation (62) possesses solutions for the following two cases:

Case I: $\psi'' \neq 0$
Case II: $\psi'' = 0$

We consider there two cases separately.

Case I:

When $\psi'' \neq 0$ the coefficients of equations (62) suggests to seek solution of the form:

$$T = \frac{K(\theta)}{r^2} \qquad \rightarrow(67)$$

Substituting equation (67) in equation (62) we get

$$K''+(2RePr\psi'+4)K=0 \qquad \rightarrow(68)$$

The solutions of (68) depends on the form of the coefficient of K, and some of them are determined as follows:

(i) When θ^m is an integral part of equation (68), we get

$$\psi = \frac{-2\theta + m(m-1)\theta^{-1}}{Re\,Pr} + b_3 \qquad \rightarrow(69)$$

$$K = \begin{cases} (b_4 \ln\theta + b_5)\theta^{\frac{1}{2}} & , m = \frac{1}{2} \\ \frac{b_4\theta^{-m+1}}{-2m+1} + b_6\theta^m & , m \neq \frac{1}{2} \end{cases} \qquad \rightarrow(70)$$

Where b_3, b_4, b_5 and b_6 are all non-zero constants.

(ii) When $Re\,Pr\,\psi'+2 = \frac{\lambda}{2\theta^2}$, the solution of equation (68) is

$$\psi = -\frac{2}{Re\,Pr} - \frac{\lambda}{2\,Re\,Pr\,\theta} + c_1 \qquad \rightarrow(71)$$

$$K = \begin{cases} (c_3 + c_3 \ln\theta)\theta^{\frac{1}{2}} \\ c_4\theta^{m_1} + c_5\theta^{m_2} \\ \theta^{\frac{1}{2}}(c_6 \cos(n \ln\theta) + c_7 \sin(n \ln\theta)) \end{cases}$$

$$,\lambda = \frac{1}{2}, m_{1,2} = \frac{1 \pm \sqrt{1-2\lambda}}{2}$$
$$,1-2\lambda > 0 \qquad \rightarrow(72)$$
$$,1-2\lambda < 0, 1-2\lambda = -n^2, n > 0$$

(iii) For $-2\,Re\,Pr\,\psi' = \theta^2$ $\rightarrow(73)$

The solution of equation (68) is

$$\psi = -\frac{\theta}{2\,Re\,Pr} + c_8 \qquad \rightarrow(74)$$

$$K = c_9 J_1(\theta) + c_{10} J_2(\theta) \qquad \rightarrow(75)$$

Where

$$J_1(\theta) = a_0\left(1 - \theta^2 - \frac{3}{4}\theta^4 + ...\right) \qquad \rightarrow(76)$$

$$J_2(\theta) = a_0\left(\theta + \frac{\theta^3}{6} + ...\right) \qquad \rightarrow(77)$$

and $a_0 \neq 0$ constant.

(iv) When $\psi' = -\frac{\lambda_1}{2\,Re\,Pr\,\theta^2}$, then

$$\psi = \frac{\lambda_1}{2\,Re\,Pr\,\theta} + c_{11} \qquad \rightarrow(78)$$

Where λ_1 $(\neq\theta)$ and c_{11} are arbitrary constants. The equation (68) utilizing equation (78), becomes

$$\theta^2 K'' + (4\theta^2 - \lambda_1)K = 0 \qquad \rightarrow(79)$$

On substituting $K = D(\theta)\sqrt{\theta}$ in equation (79), we get

$$\theta^2 D''+\theta D'+\left[4\theta^2-\left(\lambda_1+\frac{1}{4}\right)\right]D=0 \qquad \rightarrow(80)$$

which is a Bessel equation and its solution is

$$D(\theta)=c_{12}J_{\beta}(2\theta)+c_{13}J_{-\beta}(2\theta) \qquad \rightarrow(81)$$

Where

$$\beta=\sqrt{\lambda_1+\frac{1}{4}}$$

and $J_{\pm\beta}(2\theta)$ are the Bessel functions. The solution of equation (79), therefore, is

$$K=\theta^{\frac{1}{2}}\left[c_{12}J_{\beta}(2\theta)+c_{13}J_{-\beta}(2\theta)\right] \qquad \rightarrow(82)$$

Case II:

When $\psi''=0$, then

$$\psi=b_7\theta+b_8 \qquad \rightarrow(83)$$

Equations (60) and (61), using equation (83), become

$$H_r=-4b_7\sin^2\theta B_r-\frac{4b_7}{r}B \qquad \rightarrow(84)$$

$$H_\theta=4b_7B_\theta\cos^2\theta-4b_7B\sin 2\theta \qquad \rightarrow(85)$$

Proceeding in the same manner as in circular flow, we get

$$H=-4b_7\sin^2\theta B-4b_7\int\frac{Bdr}{r}+1_1 \qquad \rightarrow(86)$$

$$B=\frac{1}{r}\int f(r)dr+1_1 \qquad \rightarrow(87)$$

Where 1_1 is an arbitrary constant and f(r) is an arbitrary function. Since f(r) is an arbitrary function, μ is also arbitrary. The temperature distribution T satisfies the equation

$$r^2T_{rr}+(1-\mathrm{Re\,Pr}b_7)\,r\,T_r+T_{\theta\theta}=0 \qquad \rightarrow(88)$$

The solution of equation (88) is

$$T=\begin{cases} b_{10}\theta^2+b_{11}\theta+b_{11}r-b_{10}(r\ln r-r)+b_{12} \\ b_{13}\theta^2+b_{14}\theta+\dfrac{2b_{13}}{\mathrm{Re\,Pr}}\ln r+\dfrac{b_{14}}{\mathrm{Re\,Pr}\,b_7}r^{\mathrm{Re\,Pr}\,b_7}+b_{15} \end{cases}$$

$$,1-\mathrm{Re\,Pr}\,b_7=0$$

$$,1-\mathrm{Re\,Pr}\,b_7\neq 0 \qquad \rightarrow(89)$$

Where b_{10}, b_{11}, b_{12}, b_{13}, b_{14} and b_{15} are all non-zero arbitrary constants.

3.3 PARALLEL FLOW

For parallel flow

$$\xi=x,\ \eta=y,\ g_1=1,\ g_2=1,\ \alpha=0 \qquad \rightarrow(90)$$

Equations (30 – 38), employing equation (90), become

$$(\psi''\mu)_x-\mathrm{Re}H_y+\mathrm{Re}\psi'\psi''=0 \qquad \rightarrow(91)$$

$$(\mu\psi'')_y-\mathrm{Re}H_x=0 \qquad \rightarrow(92)$$

$$T_{xx}+T_{yy}-\mathrm{RePr}\psi'(y)T_x=0 \qquad \rightarrow(93)$$

Using $H_{xy}=H_{yx}$, to eliminate H from equations (91) and (92), we get

$$(\mu\psi'')_{xx}-(\mu\psi'')_{yy}=0 \qquad \rightarrow(94)$$

Equation (94) is the equation which the viscosity μ and the stream function ψ' must satisfy for parallel flows of an incompressible fluid of variable viscosity.

We now determine the solutions of equations (91 – 94) as follows:

On substituting

$$T=X(x)+Y(y) \qquad \rightarrow(95)$$

in equation (93), we get

$$X''+Y''-\mathrm{RePr}\psi'X'=0 \qquad \rightarrow(96)$$

Differentiating equation (96), w.r.t "x", we get

$$X''' - \mathrm{Re}\Pr\psi'(y)X'' = 0 \qquad \rightarrow(97)$$

This can be re-written as

$$\frac{X'''}{X''} = \mathrm{Re}\,\mathrm{Pr}\,\psi'(y) = b_1 \quad \text{(say)} \qquad \rightarrow(98)$$

provided $X'' \neq 0$.

The solution of equation (98) is

$$X = e^{b_1 x}\left[\int (b_3 x + b_4)e^{-b_1 x}\,dx + b_5\right] \qquad \rightarrow(99)$$

$$\psi = \frac{b_1}{\mathrm{Re}\,\mathrm{Pr}}y + b_2 \qquad \rightarrow(100)$$

Where b_1, b_2, b_3, b_4, b_5 are all non-zero constants. Equation (96), using equations (99) and (100), we get

$$Y'' + b_3 = 0 \qquad \rightarrow(101)$$

Whose solution is

$$Y = -b_3\frac{y^2}{2} + n_1 y + n_2 \qquad \rightarrow(102)$$

Where n_1 and n_2 are non-zero arbitrary constants.

When $X'' = 0$, then

$$X = b_6 x + b_7 \qquad \rightarrow(103)$$

and equation (96) yields

$$Y = \mathrm{Re}\,\mathrm{Pr}\,b_6\int\psi(y)dy + b_8 y + b_9 \qquad \rightarrow(104)$$

where $\psi(y)$ is an arbitrary function.

Let us now determine some solutions of equation (94) as follows:

(i) When $\psi'(y) = b_1 / \mathrm{Re}\,\mathrm{Pr}$, the equation (94) is identically satisfied and μ becomes an arbitrary function, and H turns out to be a constant.

(ii) When $\psi(y)$ is arbitrary, the equation (94) can be re-written as:

$$\frac{\mu_{xx}}{\mu} - \frac{\mu_{yy}}{\mu} - 2\frac{\mu_y}{\mu}\frac{\psi'''}{\psi''} - \frac{\psi^{IV}}{\psi''} = 0 \qquad \rightarrow(105)$$

The solution of this equation is determined as follows:
Differentiating equation (105) w.r.t "x", we get

$$\left(\frac{\mu_{xx}}{\mu}\right)_x - \left(\frac{\mu_{yy}}{\mu}\right)_x - 2\left(\frac{\mu_y}{\mu}\right)_x\frac{\psi'''}{\psi''} = 0\,,\ \psi''' \neq 0 \qquad \rightarrow(106)$$

This can be re-written as

$$\frac{\left(\frac{\mu_{xx} - \mu_{yy}}{\mu}\right)_x}{\left(\frac{\mu_y}{\mu}\right)_x} = 2\frac{\psi'''}{\psi''}\,,\ \left(\frac{\mu_y}{\mu}\right)_x \neq 0 \qquad \rightarrow(107)$$

Since $\psi = \psi(y)$, the equation (107) yields

$$2\frac{\psi'''}{\psi''} = l_1 \qquad \rightarrow(108)$$

and

$$\mu_{xx} - \mu_{yy} - l_1\mu_y = \mu R(y) \qquad \rightarrow(109)$$

Where l_1 ($\neq 0$) constant and R(y) is the unknown function to be determined. The solution of equation (108) is

$$\psi e^{-\frac{l_1}{2}y} = \int(l_2 y + l_3)e^{-\frac{l_1}{2}y}dy + l_4 \qquad \rightarrow(110)$$

Using equation (108) in equation (105), we get

$$\mu_{xx} - \mu_{yy} - l_1\mu_y = \frac{l_1^2}{4}\mu \qquad \rightarrow(111)$$

Comparing equations (109) and (111), we get

$$R(y) = \frac{l_1^2}{4} \qquad \rightarrow(112)$$

When $\mu = \mu(x, y)$, a solution of equation (111) is

$$\mu = \begin{cases} e^{l_5 x}(l_6 y^{n_1} + l_7 y^{n_2}) & ,l_5 \neq -\dfrac{l_1}{2}\,,\ n_{1,2} = -\dfrac{l_1}{2} \pm 5 \\ e^{l_5 x}(l_8 + l_9 y^{-l_1}) & ,l_1 = 2l_5 \end{cases} \qquad \rightarrow(113)$$

When $\mu = \mu(y)$, the solution of equation (111) is

$$\mu = (l_{10} + l_{11} y)e^{-\frac{l_1}{2}y} \qquad \rightarrow(114)$$

In equations (113) and (114) l_5, l_6, l_7, l_8, l_9, l_{10}, l_{11} are all non-zero arbitrary constants

Now when $\psi''' = 0$, then

$$\psi = l_{12}y^2 + l_{13}y + l_{14} \qquad \rightarrow(115)$$

The equation (105), employing $\psi''' = 0$, yields

$$\mu_{xx} = \mu_{yy} \qquad \rightarrow(116)$$

The solution of equation (116) is

$$\mu = l_{15}\frac{\left(x^2 + y^2\right)}{2} + l_{16}x + l_{17}y \qquad \rightarrow(117)$$

Where l_{15}, l_{16}, l_{17} are all non-zero constants.

If we assume

$$\mu = (m_1 x + m_2)Z(y) \qquad \rightarrow(118)$$

the equation (105) becomes

$$Z'' + \frac{2\psi'''}{\psi''}Z' + \frac{\psi^{IV}}{\psi''}Z = 0 \qquad \rightarrow(119)$$

Whose solution is

$$Z = \frac{m_3 y + m_4}{\psi''} \qquad \rightarrow(120)$$

Where m_3, m_4 are non-zero arbitrary constants. We note that in equation (120), the function ψ is arbitrary. The expression for the function H, in this case, is given by

$$H = \frac{m_3(m_1x + m_2)^2}{2m_1 Re} + \frac{\psi^2}{2} + \frac{m_1}{2m_3}(m_3y + m_4)^2 + m_5 \qquad \rightarrow(121)$$

Where m_5 is an arbitrary constant.

4. CONCLUSIONS

In this paper, a mathematical study of two dimensional steady flow of an incompressible Newtonian fluid of variable viscosity for an arbitrary state equation is conducted. The flow equations are transformed into (ϕ, ψ) – system with viscosity μ, the stream function ψ, the vorticity ω, the energy and transformation matrices as the unknown functions. Some exact integrals are determined for circular, redial and parallel flows. In the case of circular flow when the function $B = 0$, the viscosity μ is arbitrary, and when $B \neq 0$, the solution of the energy equation depends on the form of the coefficient of T_θ. Using some forms the coefficient of T_θ, the solutions of the energy equation are determined. The reader, by taking other forms of the coefficient, can determine more solutions of the energy function. In case of parallel flows, when μ is defined by equation (118), the stream function ψ is arbitrary and this arbitrariness ψ enables us to construct a large number of solutions to the flow equations.

REFERENCES

[1] Martin, M.H.: The flow of a viscous fluid I, Arch. Rat. Mech. Anal, 41, pp. 266-286, 1971.

[2] Nath, V. I.: On plane flows of compressible fluids. Meccanica e Fisica mathematica, Institute Lombardo (Rend. Sc.) A 108, pp. 458-476, 1974.

[3] Naeem, R.K.: On exact solution for Navier-Stokes equations, M.Sc. Major paper, Department of Mathematics and Statistics, U. of Windsor, Windsor, Canada, 1984.

[4] Naeem, R.K.: Exact solutions of the flow equations of an incompressible fluid of variable viscosity via one – parameter group, The Arabian Journal for Science and Engineering, vol. 19, No. 1, pp. 111-114, 1994.

[5] Naeem, R.K.: Steady plane flows of an incompressible fluid of variable viscosity via Hodograph transformation method, Karachi University Journal of Sciences Vol. 31, No. 1, pp. 73-89, 2003.

[6] Pinarbasi, A., and Liakopoulos, A.: The role of variable viscosity in the stability of channel flow, Int. Comm. Heat Man. Transfer, Vol. 22, No. 6 pp. 837-847, 1995.

A METHODOLOGY FOR PROCESS IMPROVEMENTS USING SPC IN A CONTINUOUS OR DISCRETE TYPE MANUFACTURING PROCESS

Abdul Sattar Jamali*, Muhammad Sharif Jamali** and Zameer Ahmed Abro***

ABSTRACT

A primary objective of statistical process control (SPC) is to maintain quality characteristics of items generated by a process as close as possible to target values for as much time, or amount of production, as possible. Customers view point and expectations have changed significantly in the past few years. Customers now do not merely expect the products to be "within specification limits". They expect, rightly so, the products to be "on target". Uniformity has become more and more important as traditional goal of "aiming to be within specifications" becomes less and less relevant. So SPC can help companies cut costs, improve quality, and pursue continuous improvement and also satisfy the customers. To move towards the achievement of this objective a methodology has been represented in this research paper. This proposed methodology has been applied in real case study of manufacturing environments. As this methodology has been applied first time in manufacturing industry, so results obtained were not satisfactory. Because the factory has never been applied statistical techniques for controlling the process, even they are not taking the significant advantages from the data collected. However, if they continuously applied this proposed methodology certainly will bring continuous improvements in their manufacturing process.

Key words: Statistical Process Control, Control Charts, Discrete and Continuous, Defective.

1. INTRODUCTION

The term "quality" is defined as any factor that enhances the value of product in the eyes of customer [1]. It is the customer whose needs are being catered to, and consequently, whose demands have to meet. This customer-oriented definition of "quality" has changed the production philosophy in manufacturing environments. It is of utmost importance to have a process operating on target. Quality control has become key part of every manufacturing process (continuous or discrete).

Control of process variability plays an important part in manufacturing because any deviation in the process and resulting product may run the risk of dissatisfying customers. Process variability is mostly measured by both mean and variance of the quality characteristic on a product part. The most implemented techniques to achieve process control are often referred to as Statistical Process Control (SPC) [2].

In this paper we have presented a methodology to improve the manufacturing process (continuous or discrete) by using SPC. The SPC is widely used process monitoring technique, especially continuous or discrete process industries, for the continuous improvements of

* Ph.D Student, School of Management and Economics, Beijing Institute of Technology, Beijing, China.
** Assistant Professor, Mehran University of Engineering & Technology, Jamshoro.
*** Assistant Professor, Quaid-e-Awam University of Engineering, Science & Technology, Nawabshah.

products and process [3]. The primary tool of SPC is Statistical Control Charts [4]. SPC in the form of control charts (e.g. Shewhart charts and Cusum charts) is useful in improving product quality by continually checking the "stable state" system. When there is a departure from 1he stable-state of statistical control (due to certain special events) and detected by control charts, the engineers or analyst then look for the assignable causes (also called special causes) and try to eliminate them [3].

Quality control techniques are critical activities in manufacturing industries when maintaining and improving product quality is a priority. In this paper we use a case study from real life in order to check 1he suitability of this proposed methodology. The remainder of this paper is organized as follows. In section 2, we presented the steps of the proposed methodology. Section 3 provides the results and discussions of the applied methodology.. Finally the section 4 related to the concluded part.

2. METHODOLOGY

The methodology represented in Fig.1 towards achievements of continuous process improvements,

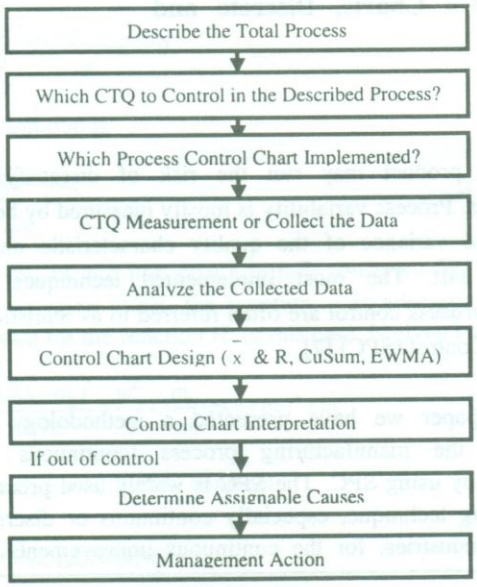

Fig.1: Methodology for Continuous Process Improvement

Following are the Steps of the Methodology,

Step-1: Studying the process of either continuous type or discrete type of process of company and identifying which product characteristics or critical characteristics or critical to quality cha.acteristics (CTQ) to control.

When SPC would be implemented by any manufacturing Industry first time, the quality engineer (practitioners) needs to study and understood all steps of manufacturing process. According to customer requirement the CTQ would be identified. In this case study, gloss acrylic resin process was chosen for analysis purpose. There are total seven steps of the processes where data has been taken at the online inspection point.

Step-2: Determine where in the process the control charts should be implemented.

After identification of CTQ at the inspection point, there is need to make decision which SPC tools would be implemented. As explained in introduction that control charts are very popular tool used in SPC. So control charts implementation decision depends on the shift in magnitude (larger and smaller) of process.

Step-3: Collecting the data for the determined process of each company.

In this case study data were collected at the inspection point covering of total 57 sample numbers in different days and samples are grouped of size 3 (n=3). This is fundamental idea of SPC that the subgroup or samples should be rational. A rational subgroup is a group in which all observations are generated under conditions in which only random effects are responsible for the observed variation. Larger subgroups have more power than smaller subgroups on Shewhart charts. On the other hand, smaller subgroups take less time to complete data collection, so significant changes may be signaled sooner.

Step-4: Analyzing the collected data to check the sufficiency of sample, the normal assumption, and randomness by applying confidence interval estimation, test of normality, and runs test of randomness.

From the collected data a global average and process standard deviation was taken. Normality assumption is very important in manufacturing process. The data may follow normal distribution. This is not always true in real case; some time data may not follow normal distribution. In this case, non-normal data would be translated to normal as formula suggested in this paper. It was explained in this paper through analytical calculations in Table 1 & 2, graphically in Figures 1, 2 & 5 for normality checking of data through by excel and Minitab quality software.

Table 1: The χ^2 (Chi-Square Test for Goodness-of-Fit for Normal Distribution of % Non-Volatile

Level	Interval	Mid-point (X_i)	Observed Frequency (O_i)	Z-lower	Z-upper	Probability $P(Zi \leq z \leq Zu)$	Expected Frequency (Ei = npi)
1	47.5-48.5	48	2	-2.91	-1.79	0.0349	1.9906
2	48.5-49.5	49	12	-1.79	-0.66	0.2179	12.4186
3	49.5-50.5	50	24	-0.66	0.46	0.4226	24.0882
4	50.5-51.5	51	17	0.46	1.58	0.2658	15.1478
5	51.5-52.5	52	2	1.58	2.71	0.0537	3.0601
Total			57			0.9948	56.7053

Level	Interval	Observed Frequency (O_i)	Expected Frequency (E_i)	$(O_i - E_i)^2 / E_i$
1	47.5-49.5	14	14.4092	0.0116
2	49.5-50.5	24	24.0882	0.0003
3	50.5-51.5	17	15.1478	0.2265
4	51.5-52.5	2	3.0601	0.3672
Total		57	56.7053	0.6057

Table 2: Histogram Calculations for % Non-Volatile Measurements on Gloss Acrylic Resin

Level	Interval	Mid-point (X_i)	Observed Frequency
1	47.5-48.5	48	2
2	48.5-49.5	49	12
3	49.5-50.5	50	24
4	50.5-51.5	51	17
5	51.5-52.5	52	2
Total			57

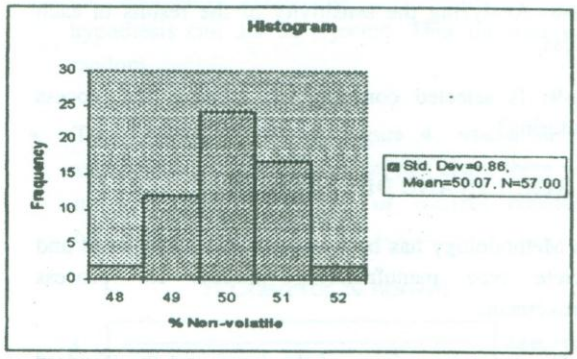

Fig. 2: The Histogram of % Non-volatile Measurement on Gloss Acrylic Resin (Table1)

Step-5: Studying how to design the $\overline{X}$ and R, the cumulative sum (CUSUM) and the exponentially weighted moving-average (EWMA) con1rol charts.

As explained in Step-2, the implementation of control charts depends on the magnitude of process shift. Process shift may be large and small from the target. When process shift is large and small, which type of control

chart is used? In this case study, as process shift was large, so it was decided to design and Implement Shewhart X-bar and R-Control charts.

Step-6: Designing the $\overline{X}$ *and R* control charts based on Shewhart control chart concept

Step-7: Designing the optimal $\overline{X}$ and R control charts.

As the data related with costs were not available, only the statistical approach was focused in this paper. In order to design a control chart, the objective was to find the combination of sample size, the control limit width at the minimum type error. For the sampling frequency, it was usually not precisely stated in this paper. With a high rate of loss from operating in an out-of-control state, the interval between samples would be small. With high inspection costs, the interval would be large. Considering the sample size, Montgomery (1997) proposes that n > = 10, the range losses efficiency very rapidly. Therefore this study only concentrates on the optimal design of X-bar and R-control charts when n == 3.

Step-8: Analyzing the sensitivity of the results in each process.

Step-9: Is selected control chart suitable for process monitoring?

3. RESULTS AND DISCUSSIONS

This Methodology has been applied in a Continuous and Discrete type manufacturing process for process improvement.

- The percent precision of the mean and the standard deviation of all data were calculated as shown in Table 3. Although the precision of the standard deviation was large, the precision percent of the mean was small. Therefore the collected data considered to be enough to estimate the value of the process parameters.

- Mostly all the control charts are based on the assumption that the universe from which a sample is drawn is normally distributed. To test the assumptions of normality, this research work used graphic methods for primary checking and conforms it by employing the χ^2 test for goodness-of-fit as follows the method shown by Ducan (1986) and Hines and Montgomery *(1990),* respectively.

- The data from Table 4 was plotted in the form of the histograms as shown in Figure 2 to check how the distributions look like. To construct the histogram, each set of data is grouped into constant intervals and the number of times in each interval is counted, the results are the frequency as distribution presented in Table 1. The graphical representation of the distribution of % non-volatile measurements on glass acrylic resin (type 1) represented in Figure, considered to be unimodel.

- From Chi-square (χ^2) test for goodness-of-fit Table 1, the calculated value of $\chi^2_{\,o} = 0.6051$ is less than table value $\chi^2_{\,0.05,1} = 3.84$ i.e. (0.6057 < 3.84). Since the 3.84 was greater than 0.6051 the null hypothesis can not be rejected at 5% significant level. Therefore the collected data was normally distributed with mean equal to 50.09 and a standard deviation equal to 0.89.

- Two approaches were used for this research work, the scatter diagram and runs test of randomness because when frequency approach applied to probability was the main concept of randomness.

  Blank (1980) recommends a scatter diagram in which a graph of the data for two variables should be plotted first to see the pattern of the data. Figure shows the scatter diagram of % non-volatile measurements on gloss acrylic resin (type 1). The scatter diagram as shown in Figure 3 shows no pattern. This feature indicates that data are random.

Table 3: 95% Confidence Interval (C.I) and the % Precision

Types of Process	Characteristics	Table	n	$\overline{X}$	S	Mean		Standard Deviation	
						CI	% Precision	CI	% Precision
Continuous or Discrete	% non-volatile	1	57	50.068	0.864	49.839 - 50.297	0.46	0.7299 - 1.0592	22.56

Table 1: % Non-Volatile Measurement on Gloss Acrylic Resin (Type 1)

Sample No.	% Non-volatile	Sample No.	% Non-volatile
1	50.0	31	50.0
2	51.0	32	50.9
3	49.0	33	50.0
4	50.0	34	49.0
5	51.0	35	50.0
6	50.0	36	50.9
7	50.9	37	51.0
8	50.0	38	50.9
9	49.0	39	50.0
10	48.0	40	49.0
11	51.0	41	50.0
12	51.0	42	50.0
13	50.0	43	51.9
14	50.0	44	48.0
15	50.0	45	50.0
16	50.0	46	50.0
17	49.0	47	49.0
18	49.0	48	50.0
19	50.9	49	49.0
20	51.0	50	50.0
21	50.0	51	50.9
22	50.9	52	50.0
23	50.0	53	50.9
24	51.0	54	52.0
25	49.0	55	50.0
26	49.0	56	50.6
27	50.9	57	49.2
28	50.0	Average 50.068	
29	49.0	S.D 0.8642	
30	51.0		

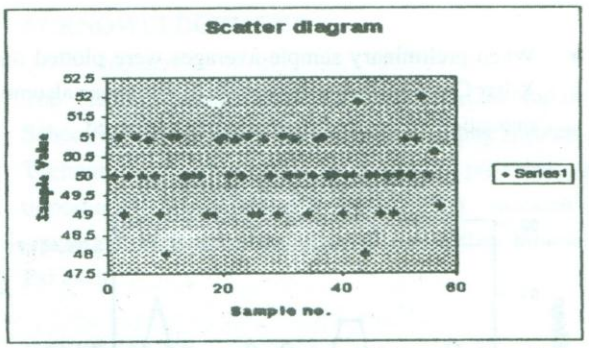

Fig. 3: The Scatter Diagram Plotted Between Sample no. VS% Non-volatile Measurements on Gloss Acrylic (Table 1)

Blank (I980) presents the runs test as a nonparametric test which is able to accept or reject a null hypothesis without knowledge of underlying population and parameters. Usually sample that taken from a population should be random. The nm test evaluates the null hypothesis. By applied the runs test to data in Table 4, the value of Z was within the acceptance region $|z| \leq 1.96$ that the null hypothesis can not be rejected. Thus the data was random.

- The R-Chart shown in Figure 4, where the 57 sample ranges were plotted on this chart, there was no indication of an out of con1rol condition observed.

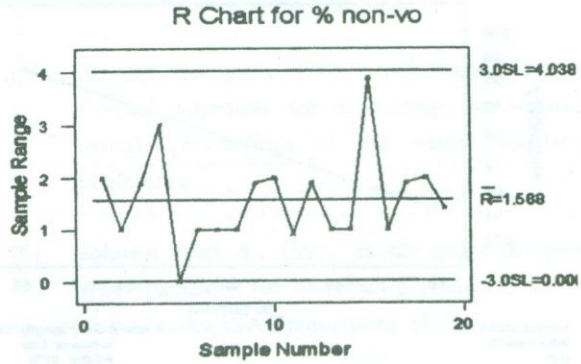

Fig. 4: The R-Chart of % Non-volatile Measurements on Gloss Acrylic Resin When n=3

- When preliminary sample averages were plotted on X-bar Chart as shown in Figure 5, there was also no indication of an out of con1rol was observed.

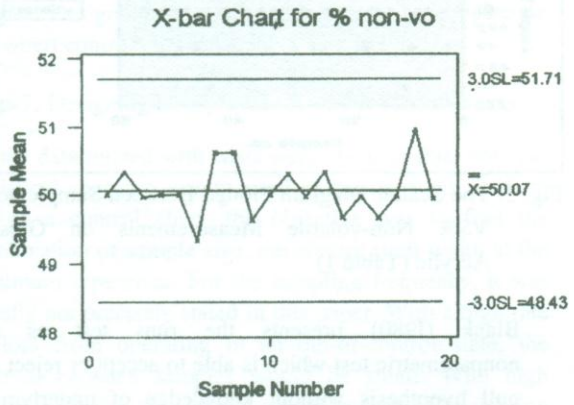

Fig. 5: The $\bar{X}$ Chart of % Non-volatile Measurements on Gloss Acrylic Resin When n=3

- The probability plot shown in Figure 6 to assess the validity of normal assumption. When all the data points show a straight line on a normal probability plot, the data presumed to be the form of normal distribution. When all data points were drawn through Minitab, the data were drawn straight line.

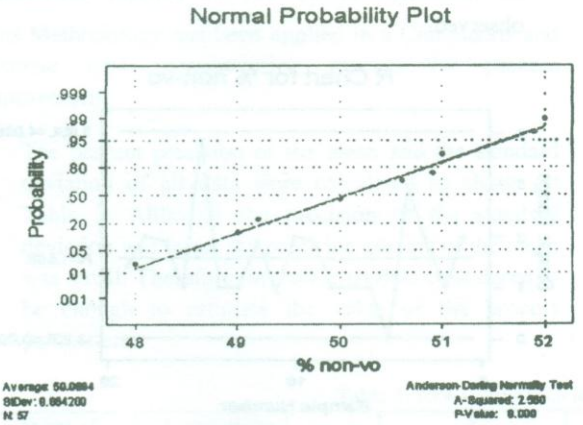

Fig. 6: Normal Probability Plot of % Non-volatile Measurements on Gloss Acrylic Resin

4. CONCLUSIONS

This paper discusses the use of statistical process control techniques systematically in a practical manufacturing environment. After the application of proposed methodology in particular manufacturing process, in a general way, it was Possible to notice that lot of defective products were produced during process and which were very costly for that company. There fore it was suggested that continuously follow this proposed methodology to that process in order to minimize the losses. Because the company never been used SPC tools even they have significant amount of data.

Based on the analysis of proposed methodology and results obtained for selected process, the conclusion are presented as follows:

- At 95 % confidence the true process mean, standard deviation lie in between limits. If the values of process mean, standard deviation lies between the limits the data are considered to be normal. If the data does not lay in between limits the data is considered to be not normal i.e. $49.8386 \leq u \leq 50.2974$ and $0.7299 \leq o \leq 1.0592$
- The Histogram plot represented that the data was normal
- Chi-square test showed the data was normally distributed on the basis of the Not rejection of null hypothesis. Incase if null hypothesis was rejected then data to be considered not normal.
- If scatter diagram showed some pattern then data may be considered not normal. But here the pattern was not random, so data was normal.

- The process shift was very large, therefore the X-bar and R-control charts were suitable.
- The sampling of data were taken in different days, but it was required that data may be taken every two hours five samples.
- Using the small sample size (n = 3), result in a relatively large be risk for detecting small shifts. However, there was good chance that the larger shifts will be detected reasonably quickly.
- A larger sample will cause the limits of a control chart to come closer to the center line on the chart with fixed value of the width of the control limits. This is because the standard deviation of the statistics X-bar and R vary inversely with the square root of sample size. Hence, the larger sample size, the smaller standard deviation, and the closer control limits will be to the center line on the chart. The effect of tighter control limits is to reduce the risk of not catching a shift in the process.
- One can design control charts and other calculations (process capability) after analyzing the data to be normal.

SUGGESTION

It is also possible practically that one could not get normal data from real or practical situation. In that case convert non normal data into normal by following formula

$$X_{Trans} = \sqrt{\frac{1}{X_{Raw}}} \quad [11]$$

Hope this methodology would be beneficial for the practitioner and educationist in order to implement SPC in a quality control practice.

ACKNOWLEDGEMENT

The Authors are grateful for data collected industry, School of Management & Economics, Beijing Institute of Technology for providing the facilities, privileges and opportunity for system analysis. This research is supported by a research grant from Higher Education Pakistan.

REFERENCES

[1] Evans, J.R. and Lindsay, W.M., 1993, "in the management and control of quality", 2nd edition, New York

[2] Chang Shing I., and Thomes R. Samuel 1998, A Control Point Methodology for Cusum control charts, Computer Ind. Engng. Vo134, No.3, pp. 565-572.

[3] Harriet Black Nembhard, Kao Ming-shu, Lim Gino., 1999, Integrating Discrete event simulation with statistical process control charts for transitions in a manufacturing environment, Proceedings of the winter simulation conference.

[4] Chen Yan-Kwang, Liao Hung-chang. 2004, Multi-criteria design of an X Control Chart, Computers and Industrial Engineering 46, 877-891.

[5] Stewart Robinson, 2002, A Statistical Process Control approach for estimating the warm-up period, proceedings of the winter simulation conference.

[6] Jokinen Petri A., 1995, on the usage of spread sheet packages for automating statistical process control tasks, ISA Transactions 34,29-37.

[7] Pankaj Jalote, Saxena Ashish., December 2002, Optimal Control Limits for employing statistical

process control in software process, IEEE Transactions on software engineering, vo128, No.12.

[8] Hayer and Ellis, November 1996, an other look at .. "A Graphical Exploration of SPC", Quality Progress, pp.85-93.

[9] Joseph J. Pignatiello. JR, and Thomas R Samue1. January 2001. Estimation of the change point of a normal process mean in SPC application, Journal of Quality Technology. V. 33. No.1. pp.82-95.

[10] Montgomery. D.C.. 1997. Introduction to Statistical Quality Contro1. 3rd edition. wiley. New York

[11] Mikal J. Harry. Ph.D. 1997. Six-Sigma Statistics. The Vision of Six-Sigma: Tools and Methods for Break Through. 5th edition.

SOME EXACT SOLUTIONS TO EQUATIONS OF MOTION OF A THIRD GRADE FLUID FOR SELECTED VORTICITY

Rana Khalid Naeem*, Waseem Ahmed Khan** and Sultan Hussain**

ABSTRACT

Some exact solutions of the equations governing the steady plane flows of an incompressible third grade fluid for some selected forms of the vorticity are determined by using complex variables and complex functions. Some of the solutions admit, as particular cases, all the solutions of Moro , Siddqui and Kaloni [1].

Key words: Exact solutions, third grade fluid, complex variable technique, steady plane flows. MSC code. 76AO5.

1. INTRODUCTION

Recently Moro, Siddiqui and Kaloni [1] have determined some exact solutions of the equations governing the steady plane motion of an incompressible fluid of third grade employing hodograph and Legendre transformations. Moro et al transformed the basic flow equations in the hodograph plane by interchanging the dependent and independent variables. Then by defining a Legendre-transformation function of the stream function recast all the equations interms of this function. They determined the condition which Legendre-transform function of the stream function must satisfy employing the integrability condition, and obtained solutions to the flow equations by assuming forms of the function. The third grade fluid have been studied successfully for various types of flow situations. We mention here some of such studies such as [2-5] .

In this paper, we reconsider their flow equations with the objective of determining some exact solutions. To achieve our objective, in section (2) we obtain the expression for the vorticity function w, the stream function in terms of the complex variables and complex functions. Employing the compatibility condition for the generalized energy function h, we determine the condition which the complex functions must satisfy. In section (3), we determine some analytical solutions. We mention that the solutions presented in this paper admit, as particular cases, all the solutions of Moro, Siddiqui and Kaloni [1] by appropriately choosing the complex functions or the arbitrary constants therein.

2. FLOW EQUATIONS

The equations governing the unsteady motion of an incompressible fluid of third grade are

$$\text{div } V = 0 \qquad \rightarrow(1)$$

$$\rho \frac{dV}{dt} = \rho F + \text{div} T \qquad \rightarrow(2)$$

where V is the velocity vector, ρ the density, and F the body forces .The cauchy stress tensor T for an incompressible third grade fluid is characterized by the constitutive equations

* Department of Mathematics & Basic Sciences, NED University of Engineering & Technology, Karachi.

** Department of Mathematics, University of Karachi, Karachi.

$$T = - pI + \mu A_1 + \alpha_1 A_2 + \alpha_2 A_1^2 + \beta_1 A_3 + \beta_2 (A_1 A_2 + A_2 A_1) + \beta_3 (\text{tr } A_1^2) A_1 \quad \rightarrow (3)$$

In equation (3), p is the pressure, I the unit tensor, and A_1, A_2, and A_3 are the first three Rivlin-Ericken tensors defined as

$$A_1 = \nabla V + (\nabla V)^T \quad \rightarrow (4)$$

$$A_2 = \frac{dA_1}{dt} + A_2 (\nabla V) + (\nabla V)^T A_1 \quad \rightarrow (5)$$

and

$$A_3 = \frac{dA_2}{dt} + A_2 (\nabla V) + (\nabla V)^T A_1 \quad \rightarrow (6)$$

where $\frac{d}{dt}$ the material time derivative.

For a steady plane motion in xy- plane ,the equations (1) and (2) , in the absence of body forces, reduce to

$$u_x + V_y = 0 \quad \rightarrow (7)$$

$$h_x = \rho v w - \mu w_y - \alpha_1 v \nabla^2 w - \beta_3 (wM)_y + 2 \beta_3 \{(u_x M_x + v_x M_y)\} \quad \rightarrow (8)$$

$$h_y = - \rho u w + \mu w_x + \alpha_1 u \nabla^2 w + \beta_3 (wM)_x + 2 \beta_3 \{(u_y M_y + v_y M_y)\} \quad \rightarrow (9)$$

where

$$w = v_x - u_y \quad \rightarrow (10)$$

$$h = \frac{\rho q^2}{2} - \alpha_1 (u \nabla^2 u + v \nabla^2 v) - \frac{M}{4} (3\alpha_1 + 2\alpha_2) + p \quad \rightarrow (11)$$

$$M = 4(u_x)^2 + 4(v_y)^2 + 2(v_x + u_y)^2 \quad \rightarrow (12)$$

$$q^2 = u^2 + v^2 \quad \rightarrow (13)$$

Equations (7-9) are three non-linear partial differential equations for three unknowns u, v and p as functions of (x,y).

In obtaining equations (8), (9) and (11), it has been taken into considerations that the viscosity u and the material constants α_1, α_2, β_1, β_2, β_3, satisfy the following constraints [6,7]

$$\mu \geq 0 \, , \alpha_1 \geq 0 \, , \beta_1 = \beta_2 = 0, \beta_3 \geq 0,$$

$$- \sqrt{24 \mu \beta_3} \leq (\alpha_1 + \alpha_2) \leq \sqrt{24 \mu \beta_3}$$

Equation (7) implies the existence of a stream function $\Psi(x,y)$ such that:

$$u = \Psi_y, \qquad v = - \Psi_x \quad \rightarrow (15)$$

Equations (8) and (9), on utilizing the equation (15) and the compatibility condition $h_{xy} = h_{yx}$, yield

$$\rho [\Psi_y w_x - \Psi_x w_y] - \mu \nabla^2 w - \alpha_1 [\Psi_y (\nabla^2 w)_x - \Psi_x (\nabla^2 w)_y] - \beta_3 [(w M)_{xx} + (w M)_{yy}] + 2\beta_3 [2 \Psi_{xy} M_{yx} - \Psi_{xx} M_{yy} - \Psi_{yy} M_{xx}] = 0 \quad \rightarrow (16)$$

Where

$$w = - (\Psi_{xx} + \Psi_{yy}) \quad \rightarrow (17)$$

$$M = 8 \Psi^2_{yx} + 2 (\Psi_{yy} - \Psi_{xx})^2 \quad \rightarrow (18)$$

Let

$$Z = x + i y, \qquad z = x - i y \quad \rightarrow (19)$$

Then from Naeem and Stallybrass [8,9]:

$$2 (\bullet)_{\bar{z}} = (\bullet)_x + i (\bullet)_y \, , \qquad 2 (\bullet)_z = (\bullet)_x - i (\bullet)_y$$

$$4 \text{Im}[(\bullet)_{\bar{z}} (o)_z] = (\bullet)_y (o)_x - (\bullet)_x (o)_y \quad \rightarrow (20)$$

Where the notations $\bullet$, $\bullet$, o, represent flow variables of

interest. Equations (8), (9) and (16), on utilizing equation (20), become

$$h_z = (v+iu)\frac{J}{2} - iL_z + 2\beta_3[u_z(M_z + M_{\bar{z}}) + iv_z(M_z - M_{\bar{z}})] \quad \rightarrow(21)$$

$$h_{\bar{z}} = (v+iu)\frac{J}{2} + iL_{\bar{z}} + 2\beta_3[u_{\bar{z}}(M_z + M_{\bar{z}}) + iv_{\bar{z}}(M_z - M_{\bar{z}})] \quad \rightarrow(22)$$

$$\mathrm{Im}\,[\Psi_{\bar{z}}\,(\rho w_z - 4\alpha_1 w_{zz\bar{z}})] - \mu\, w_{z\bar{z}}\beta_3\,(w_{z\bar{z}}M + w_z M_{\bar{z}} + w_{\bar{z}} M_z) + 2\beta_3\,(\Psi zz\, M_{\bar{z}\bar{z}} + \Psi_{\bar{z}\bar{z}} M_{\bar{z}\bar{z}}) = 0 \quad \rightarrow(23)$$

Where

$$J = \rho w - 4\alpha_1 w_{z\bar{z}}$$

$$L = \mu w + \beta_3 w M$$

$$u = i\,(\Psi_z - \Psi_{\bar{z}})$$

$$v = -\,(\Psi_z + \Psi_{\bar{z}})$$

3. SOLUTIONS

On integrating the fifth equation in equation (24), we obtain

$$\Psi = -\iint \frac{w}{4} dz d\bar{z} + A + A^* \quad \rightarrow(25)$$

where A and A* are complex functions and A* is the complex conjugate of A. To determine the solution of equation (23), our strategy will be to specify the vorticity function w and determine the condition which the functions A and A* must satisfy. The condition is obtained from equation (23) utilizing equation (25).

I. When the vorticity is zero, the equation (25) yields

$$\Psi = A + A^* \quad \rightarrow(26)$$

Equation (23), on utilizing Equation (26), yields

$$\beta_3\,(A''^2\, A^{*IV} + A^{*''2}\, A^{IV}) = 0,\ A'' \neq 0,\ A^{*''} \neq 0 \quad \rightarrow(27)$$

When $\beta_3 \neq 0$, then equation (27) has two solutions

$$A = a\, i\, \ln z \quad \rightarrow(28)$$

and

$$A = \frac{a_1}{6}z^3 + \frac{a_2}{2}z^2 + a_3 z + a_4 \quad \rightarrow(29)$$

Where a_1 is a real constant and a, a_2, a_3 and a_4 are complex constants.

The generalized energy function h for A given by equations (28) and (29) are respectively given by

$$h = \left(\frac{256}{3}\right)\frac{\beta_3 a^4}{z^3 \bar{z}^3} h_o \quad \rightarrow(30)$$

$$h = h_1 \quad \rightarrow(31)$$

In equations (30) and (31) h_o and h_1 are arbitrary real constants. In computing the generalized energy function h for given A by equation (29), the constant a_1 turns out to be zero. If we choose appropriately the constants a, a_2 and a_3, we get solutions of Moro, Siddiqui and Kaloni [1]. The pressure p can easily be obtained from equation (11) using the above expressions for h.

II. When vorticity w is constant say W_0, then equation (25) yields

$$\psi = -\frac{w_0}{4} z\bar{z} + A + A^* \quad \rightarrow(32)$$

Equation (23), on utilizing Equation (32), yields

$$\beta_3\,(A''^2\, A^{*IV} + A^{*''2}\, A^{IV}) = 0\ ,\ A'' \neq 0,\ A^{*''} \neq 0 \quad \rightarrow(33)$$

When $\beta_3 \neq 0$, then equation (33), yields

$$A = \frac{a_1}{6}z^3 + \frac{a_2}{2}z^2 + a_3 z + a_4 \quad \rightarrow(34)$$

interest. Equations (8), (9) and (16), on utilizing equation (20), become

$$h_z = (v+iu)\frac{J}{2} - iL_z + 2\beta_3[u_z(M_z + M_{\bar{z}}) + iv_z(M_z - M_{\bar{z}})] \quad \rightarrow(21)$$

$$h_{\bar{z}} = (v+iu)\frac{J}{2} + iL_{\bar{z}} + 2\beta_3[u_{\bar{z}}(M_z + M_{\bar{z}}) + iv_{\bar{z}}(M_z - M_{\bar{z}})] \quad \rightarrow(22)$$

$$\text{Im}\,[\Psi_{\bar{z}}\,(\rho w_z - 4\alpha_1 w_{zz\bar{z}})] - \mu\, w_{z\bar{z}}\beta_3\,(w_{z\bar{z}}M + w_z M_{\bar{z}} + w_{\bar{z}} M_z) + 2\beta_3\,(\Psi zz\, M_{\bar{z}\bar{z}} + \Psi_{\bar{z}\bar{z}} M_{\bar{z}\bar{z}}) = 0 \quad \rightarrow(23)$$

Where

$$J = \rho w - 4\alpha_1 w_{z\bar{z}}$$

$$L = \mu w + \beta_3 w M$$

$$u = i\,(\Psi_z - \Psi_{\bar{z}})$$

$$v = -\,(\Psi_z + \Psi_{\bar{z}})$$

3. SOLUTIONS

On integrating the fifth equation in equation (24), we obtain

$$\Psi = -\iint \frac{w}{4} dz d\bar{z} + A + A^* \quad \rightarrow(25)$$

where A and A* are complex functions and A* is the complex conjugate of A. To determine the solution of equation (23), our strategy will be to specify the vorticity function w and determine the condition which the functions A and A* must satisfy. The condition is obtained from equation (23) utilizing equation (25).

I. When the vorticity is zero, the equation (25) yields

$$\Psi = A + A^* \quad \rightarrow(26)$$

Equation (23), on utilizing Equation (26), yields

$$\beta_3\,(A''^2\, A^{*IV} + A^{*''2}\, A^{IV}) = 0,\ A'' \neq 0,\ A^{*''} \neq 0 \quad \rightarrow(27)$$

When $\beta_3 \neq 0$, then equation (27) has two solutions

$$A = a\, i\, \text{lnz} \quad \rightarrow(28)$$

and

$$A = \frac{a_1}{6}z^3 + \frac{a_2}{2}z^2 + a_3 z + a_4 \quad \rightarrow(29)$$

Where a_1 is a real constant and a, a_2, a_3 and a_4 are complex constants.

The generalized energy function h for A given by equations (28) and (29) are respectively given by

$$h = \left(\frac{256}{3}\right)\frac{\beta_3 a^4}{z^3\bar{z}^3} h_o \quad \rightarrow(30)$$

$$h = h_1 \quad \rightarrow(31)$$

In equations (30) and (31) h_o and h_1 are arbitrary real constants. In computing the generalized energy function h for given A by equation (29), the constant a_1 turns out to be zero. If we choose appropriately the constants a, a_2 and a_3, we get solutions of Moro, Siddiqui and Kaloni [1]. The pressure p can easily be obtained from equation (11) using the above expressions for h.

II. When vorticity w is constant say W_0, then equation (25) yields

$$\psi = -\frac{w_0}{4} z\bar{z} + A + A^* \quad \rightarrow(32)$$

Equation (23), on utilizing Equation (32), yields

$$\beta_3\,(A''^2\, A^{*IV} + A^{*''2}\, A^{IV}) = 0\,,\ A'' \neq 0,\ A^{*''} \neq 0 \quad \rightarrow(33)$$

When $\beta_3 \neq 0$, then equation (33), yields

$$A = \frac{a_1}{6}z^3 + \frac{a_2}{2}z^2 + a_3 z + a_4 \quad \rightarrow(34)$$

where a_1 is a real constant and all other a_i's are all complex constants. We mention here that there are other solutions of equation (33) and solution in equation (34) is the only solution that gives constant vorticity. The velocity components u and v are given by

$$u = iw_0\frac{z-\bar{z}}{4} + i\left[\frac{a_1z^2 - \bar{a}\bar{z}^2}{2}\right] + a_2z - \bar{a}_2\bar{z} + a_3 - \bar{a}_3$$

$$v = \frac{w_0}{4}(z+\bar{z}) - \left[\frac{a_1z^2 + \bar{a}_1\bar{z}^2}{2}\right] + a_2z + \bar{a}_2\bar{z} + a_3 + \bar{a}_3 \quad \rightarrow(35)$$

Equation (32), on utilizing equation (34), yields

$$\psi = -\frac{w_0z\bar{z}}{4} + \frac{\bar{a}_1\bar{z}^3 + a_1z^3}{6} + \frac{a_2z^2 + \bar{a}_2\bar{z}^2}{2} + (a_3z + \overline{a_3z}) + a_4 + \bar{a}_4 \quad \rightarrow(36)$$

Function A becomes arbitrary. The arbitrariness of A enables us to construct a large number of stream function Ψ and hence a large number of solutions to the flow equations .In this case the generalized energy function h is $-\rho\Psi\omega_0$+ constant. Furthermore, if we take the function A equal to $(c_1 + i\ c_2)\ z^2$ or $(c_2 + i\ c_3)$ ln z and choose appropriately the constants or apply the appropriate boundary conditions we get the plane coutte flow, the flow due to a spiral vortex at the origin and the flows having streamlines as a family of ellipses, concentric circles, rectangular hyperbolae. The expression for the generalized energy function h, for Ψ given by the equation (36), is

$$h = -\rho w_0\psi + \frac{128}{3}i\beta_3(a_1z + a_z)^3 - \frac{128}{3}i\beta_3(a_1\bar{z} + \bar{a}_z)^3 + h_2 \quad \rightarrow(37)$$

where h_2 is a real arbitrary constant. The pressure p can easily be obtained from equation (11).

III. When w is non-constant, the solutions of equation (23) are determined as follows:

(i) When $w = m_1 z + \bar{m}_1\bar{z}$, the equation (23) yields

$$\mathrm{Im}\left[-\frac{m_1^2z^2}{8} + m_1A^{*'}\right] = \lambda[2m_1\bar{m}_2(m_1z + \bar{m}_1\bar{z}) - 8(m_1^2A^{*'} + \bar{m}_1^2A''$$

$$-16(m_1^2\bar{z}A^{*''} + \bar{m}_1^2zA'') + 64(m_1A''A^{*'''} + \overline{m_1}A^{*''}A'')$$

$$-4(m_1^2\bar{z}^2A^{*IV} + \bar{m}_1^2z^2A^{IV}) + 32(m_1\bar{z}A''A^{*IV} + \bar{m}_1^2zA^{*'''}A^{IV})$$

$$-64(A''^2A^{*''2}A^{IV})] \quad \rightarrow(38)$$

where $\lambda = \frac{\beta_3}{4}$ and $m_1$is a complex constant.

The L.H.S of equation (38) suggests to assume

$$A^{*'} = \lambda_1\bar{z}^2 + \lambda_2\bar{z} + \lambda_3$$

which on putting in equation (38), gives

$$\lambda_1 = -\frac{\bar{m}_1^2}{8m_1}, \lambda_2 = 48\lambda 8\lambda + i24\lambda 2\xi^2 - \eta^2), \lambda_3 = d_1 + id_2, m_1 = \xi + i\eta$$

and

$$\eta d_1 + \xi d_2 = -2072\lambda^2\xi\eta(\xi^2 - \eta^2)$$

The solution of equation (38), therefore, is

$$A = \frac{\bar{\lambda}_1z^3}{3} + \frac{\bar{\lambda}_2z^2}{2} + \bar{\lambda}_3z + \bar{\lambda}_4 \quad \rightarrow(39)$$

where m_2 is a complex constant.

Equation (25), using (39) becomes

$$\Psi = -\frac{z\bar{z}}{8}(m_1z + \bar{m}_1\bar{z}) + \frac{1}{3}(\lambda_1\bar{z}^3 + \bar{\lambda}_1z^3) + \frac{1}{3}(\lambda_2\bar{z}^2 + \bar{\lambda}_2z^2)$$

$$+ (\lambda_3\bar{z} + \overline{\lambda_3z}) + \lambda_4 + \bar{\lambda}_4 \quad \rightarrow(40)$$

The expression for the generalized energy function h is too long and we do not given it here. The interested reader

can easily determine it using equations (21) and (22).

(ii) For $w = B(z + \bar{z})$, the constant B being real, the equation (23) becomes

$$\mathrm{Im}\left[-\frac{Bz^2}{8} + A^{*'}\right] = \lambda\begin{bmatrix} 2B^2(z+z) - 8B(A^{*'} + A'') - 16B(\bar{z}A^{*''} + zA^{''}) \\ + 64(A''\,A^{*''} + A^{*''}\,A^{''}) - 4B(\bar{z}^2 A^{*IV} + z^2 A^{IV}) \\ + 32(\bar{z}A''\,A^{*IV} + zA^{*''}\,A^{IV}) - 64(A''^2\,A^{*IV} + A^{*''2}\,A^{IV})/B \end{bmatrix} \rightarrow (41)$$

The L.H.S of equation (41) suggests that $A^{*'}$ should be a polynomial of degree two in z and therefore on substituting

$$A^{*'} = l_1\bar{z}^2 + l_2\bar{z} + l_3$$

in equation (41), we get

$$l_1 = -\frac{B}{8}, l_2 = 24\lambda B^2 i \text{ and } l_3 = 0 \qquad \rightarrow (42)$$

Hence

$$A^{*} = -\frac{B\bar{z}^3}{24} - 12\lambda B^2 i\bar{z}^2 + m_3 \qquad \rightarrow (43)$$

where m_3 is an arbitrary complex constant.
Using equation (43), equation (25) implies,

$$\psi = -\frac{Bz\bar{z}}{8}(z+\bar{z}) - \frac{B\bar{z}^3}{24} - 12\lambda B^2 i\bar{z}^2 - \frac{Bz^3}{24} + 12\lambda B^2 iz^2 + m_3 + \bar{m}_3$$

The generalized energy function h is given by

$$h = \frac{\rho B}{2}\left[\frac{B}{8}\frac{(z+\bar{z})^4}{4} - 24\lambda i B_2\frac{(z+\bar{z})^3}{3}\right] - i\rho Bz - 584\lambda\beta_3 B^4\frac{(z+\bar{z})^2}{2} + \rho iB\bar{z} + h_3 \qquad \rightarrow (44)$$

where h_3 is an arbitrary real constant.

(iii) When $w = D(z + \bar{Z} + E)$, D and E being real, the equation (23) yields.

$$\mathrm{Im}\left[-\frac{Dz^2}{8} - \frac{DEz}{4} + A^{*'}\right] = \lambda\begin{bmatrix} 2D^2(z+\bar{z}) - 8D(A^{*''} + A'') - 16D(\bar{z}A^{*''} + zA^{''}) \\ + 64(A''\,A^{*''} + A^{*''}\,A^{''}) - 4D(\bar{z}^2 A^{*IV} + \bar{z}^2 A^{IV}) \\ - 64(A''^2\,A^{*IV} + A^{*''2}\,A^{IV})/D + 32(\bar{z}A''\,A^{*IV} + zA^{*''}\,A^{IV}) \end{bmatrix} \rightarrow (45)$$

Following the same procedure as that of previous case we find

$$A^{*} = -\frac{D\bar{z}^3}{24} + \frac{K_2}{2}\bar{z}^2 + K_3 z + m_4 \qquad \rightarrow (46)$$

where

$$K_2 = -\frac{DE}{4} + \frac{168\beta_3 D^2}{\rho}i$$

$$K_3 = K_{31} + \frac{12D^2E\beta_3}{\rho}i$$

and m_4 is an arbitrary complex constant, and K_{31} is a real constant.

The equation (25), on using equation (46), yields

$$\psi = -\frac{Dz\bar{z}(z+\bar{z}+2E)}{8} - \frac{D}{24}(z^3+\bar{z}^3) - \frac{DE}{8}(z^2+\bar{z}^2) + \frac{168\beta_3 D^2}{\rho}i(\bar{z}^2 - z^2) + K_{31}(z+\bar{z}) + \frac{12D^2E\beta_3}{\rho}i(z-\bar{z}) + m_4 + \bar{m}_4 \qquad \rightarrow (47)$$

The equations (21) and (22) yields

$$h = 2\rho\left[(z+\bar{z})^4 + 2E(z+\bar{z})^3 + (E^2 - 2K_{31})(z+\bar{z})^2 - 2K_{31}E(z+\bar{z})\right] + 2i\mu(z-\bar{z}) + h_4$$

provided D = 2 and $\beta_3 = 0$. In equation (48), h_4 is an arbitrary real constant.

(iv) For $w = B\ln(z\,\bar{z}) + D_1$

the equation (23) is satisfied provided

$$A^* = m_6 \ln \bar{z} + m_7 \qquad \rightarrow (49)$$

where m_6, B, D_1, are real constants and m_7 is complex arbitrary constant.

The stream function Ψ for A^* given by equation (49) is

$$\psi = \frac{(-B\bar{z}z + 4m_6)\ln(\bar{z}z)}{4} + \frac{2B - D_1}{4}\bar{z}z + m_7 + \bar{m}_7 \qquad \rightarrow (50)$$

where $\bar{m}_7$ is the complex conjugate of m_7. This stream function represents the motion whose streamlines are concentric circles with speed constant along each streamlines for the appropriate choice of the constants. The generalized energy function h, in this case, is given by

$$h = \rho\left[\left(\frac{B^2}{4}z\bar{z} - m_6 B\right)(\ln z\bar{z})^2\right] + \left[-\frac{\rho B}{2} - \frac{\rho B^2}{4} + \frac{D_1 B\rho}{2}\right]$$

$$z\bar{z}\ln z\bar{z} + \left(-\frac{\rho}{2} + \frac{B^2}{2}\rho - D_1 B\rho\rho\right)\bar{z} +$$

$$\rho\left[-m_6 D_1 \ln z\bar{z} - (BD_1 - D_1^2)(z + \bar{z})^2\right]$$

$$+ 2B\mu i \ln\left(\frac{z}{\bar{z}}\right) + \left(\frac{\rho D_1 B}{8} - \frac{\rho D_1^2}{16}\right)(z - \bar{z})^2 + h_5 \qquad \rightarrow (51)$$

where h_5 is an arbitrary real constant.

4. CONCLUSIONS

The vorticity function w and the stream function Ψ are expressed in terms of the complex variables and complex function. The condition which the complex functions must satisfy is determined through the equations for the function h by using the compatibility condition $h_{xy}=h_{yx}$. Some exact solutions to the flow equations are determined using the condition for the complex functions for some selected forms of the vorticity. Some of the solutions admit, as particular cases, all the solutions of Moro, Siddiqui and Kaloni [1]. The plane couette flow, the flow due to a spiral vortex at the origin and the flows having streamlines as a family of ellipses, concentric circles, rectangular hyperbolae are also indicated.

REFERENCES

[1] Moro,L., Siddiqui, A.M., Kaloni, P.N.: Steady Flows of a Third Grade Fluid by Transformation Methods, ZAMM,Vol.70,No.3,pp.189- 198,1990.

[2] Hayat,T., Asghar, S., Siddiqui, A.M.: unsteady flow of an oscillating porous disk and a fluid at infinity, Mecanica, vol.34 ,pp.259-262,1999.

[3] Hayat ,T. , Nadeem ,S. , Asghar, A.,Siddiqui , A.M.: fluctuating flow of a third grade fluid on a porous plate in a rotating medium, Int. J. Non-linear Mechanics, vol.36, No.6 ,pp.901-916 , 2001.

[4] Akyildiz, F.T. : A note on the flow of a non-Newtonian fluid film ,Int. J. Non-Linear Mechanics, vol.33 ,No.6, pp.1061- 1069,1998.

[5] Hayat ,T. , Kara, A.H., Momoniat, E.: exact flow of a third grade fluid on a porous wall, Int. J. Non - Linear Mechanics, vol.38 , No. 6,pp.1533 - 1537,2003.

[6] Truesdell,C. , Noll, W., The non-linear field theories of mechanics. In: Handbuch der physik. vol.111 /3, Springer, Berlin, pp .494-513, 1965.

[7] Fosdick,R.S , Rajagopal, K.R.: Thermodynamics and stability of fluids of third grade. Proc. R. Soc. Lend A. 339, pp. 351 - 377, 1980.

[8] Stallybrass,M.P.: A class of exact solution of the Navier - Stokes equations. Plane unsteady flow - Lett. Appl. Engg. Sci., vol.21, No.2, pp. 179 -186, 1983.

[9] Naeem,R .K. : Some exact solutions to equations of Motion of an incompressible second grade fluid. Applied Mechanics and Engineering, vol.1, No.3, pp .435 - 444,1996.

NICKEL STEEL ROLLING PROBLEMS

Muhammad Hayat Jokhio*, Muhammad Ibrahim Panhwar** and Moinuddin Ali Khan***

ABSTRACT

The main objective of the present work is to study the nickel steels rolling process and investigate the causes of scaling and distortion problem occurring in hot rolled nickel steel plates as produced by the peoples steel mill. For this purpose the study concerned with causes of scaling and distortion were investigated during the steel processing at Peoples Steel Mills and its effect on microstructure and mechanical properties were also investigated. Tensile and hardness test were carried out to determine tensile strength, yield strength, % elongation, hardness of the rolled plates using universal tensile machine and Brinell hardness testing machine. The metallographic investigation was also carried out to investigate the effect of heat treatment on micro-structural constituents in water quenched and tempered nickel steel plate samples. Experimental results indicate that high temperature processing and uncontrolled process parameters were the major causes for scaling and distortion, which effect the performance of nickel steels.

1. INTRODUCTION

Addition of nickel to structural steel results in an increase of strength, without proportionality great decrease of ductility. Nickel lowers the critical temperatures of steel, widens the temperature range for successful heat treatment, retards the decomposition of austenite, & does not form any carbide, which might be difficult to dissolve during austenitizing [1]. Nickel also reduces the carbon content of the eutectoid; therefore the structure of unhardened nickel steels contains a higher percentage of pearlite than similarly treated plain carbon steels [2]. Since the pearlite forms at a lower temperature, it is finer & tougher than the pearlite in alloyed steels. These factors permit the attainment of given strength levels at lower carbon contents, thus increasing toughness, plasticity & fatigue resistance. Nickel steels are highly suited for high-strength structural steels, which are used in the as rolled conditions or for large forgings. Because nickel does not combine with carbon, heat-treaters may work to lower case carbons in the processing of nickel steels [3]. Since there is less likelihood of carbon being tied up in carbides, the availability of case carbon for hardening is increased. Lower transformation temperatures of nickel steels allow greater flexibility in heat treatment. Response to hardening is more uniform & lower quenching temperatures can result in less distortion [4]. Nickel steels are widely used for manufacturing gears, cam & crankshafts, bevel shafts, turbine shafts, axels, connecting rods, crown wheels, studs, gudgeon pins & for heavy-duty applications [6-8]. Nickel steel was produced & cast into slabs. Then these slabs were rolled in two high reversing mills to achieve the required thickness of the plates. Before rolling the slabs were heated in 9-ton per hour pusher type reheating furnace & then discharged from the furnace for rolling. Due to heating & exposing into open

* Associate Professor, Department of Metallurgy and Materials Engineering, MUET, Jamshoro.
** Professor, Department of Mechanical Engineering, MUET, Jamshoro.
*** General Manager Quality Control Peoples Steel Mills Karachi.

atmosphere the oxide layer was produced on the surface of slab which is called as scaling. Before rolling, the scale formed on the surface of slab should be removed, but scale formed incase of nickel steel was sticky scale. Sticky scale caused problems during rolling & produced a defective plate product containing pits & small cracks. So, for avoiding the sticky scale problems, & producing the defect free plates various coatings were applied on the surface of the slabs. Initially the slab was coated with aluminum & then with redoxine but due to high temperatures these coatings were not effective. Then coating of "graphite powder" with sodium silicate (Na_2SiO_4) was applied on the surface of slab, which gave the better results in rolled plates. After coating, the slabs were rolled by making continuous successful passes through the rolls to achieve the required thicknesses of the plates (12, 30, 40, 45 mm). For achieving required microstructure & hardness, the rolled plates were quenched in water & then tempered to relieve the thermal stresses. Due to quenching of plates in water, the plates were become uneven & some waves produced in the rolled plates. For removing the unevenness or for straightening of plates some mechanical work was adopted [9,10]. After straightening various tests like tensile test, hardness test & folding test were carried out on the quenched & tempered plates for achieving the required results in the plates. Finishing was the last step for the nickel steel plates, where the plates were grinded & sent for storage purpose. The detail of the experimental work is given as under: Automobile gears and axles, roller skates, and many machine and structural components are made of alloy steels.

2. EXPERIMENTAL PROCEDURE FOR MANUFACTURING OF NICKEL STEEL

Experimental procedure consists manufacturing of nickel steel, using electric arc furnace melting and alloying. The nickel steel was cast into slabs (ingots) & then annealed at 650°c. After annealing, the slabs were heated at 1200°c for rolling. After rolling, the plates were quenched in water to achieve the desired microstructure & properties. Then these plates were tempered for removing the thermal stresses.

2.1 MANUFACTURING STEPS

Nickel steel was manufactured by charging the scrap in the electric arc furnace (EAF). In electric arc furnace the scrap was melted & dephosphorised & alloying additions were also made in electric arc furnace. Then the molten metal was transferred to ladle furnace through ladle where desulphurization & final alloying was carried out to achieve the required composition of steel as given in the Table (1). From the ladle furnace the molten metal was shifted to vacuum degassing (VD) for the removing the gases from the molten metal by creating the vacuum into the ladle. After degassing the molten metal was cast into flat molds, & after solidification the slabs of 1250kg weight were stripped off from the molds.

Table 1: Composition of Nickel Steel

Elements	%Composition max	% Composition min
C	0.15	0.12
Si	0.25	0.20
Mn	0.50	0.45
P	Less than 0.015	-
S	Less than 0.01	-
Cr	0.50	0.45
Mo	0.40	0.30
Ni	4.7 -4.8	4.30
V	0.09	-
Cu	Less than 0.25	-
Al	0.02 - 0.03	-
Sn	Less than 0.025	-

2.2 ANNEALING OF THE SLABS

After being removed from the molds, the slabs were placed in a furnace for stress relieving annealing. The slabs were charged in the furnace in hot condition at about 400°c & heated to 660°c at the heating rate of about 20°c per hour [11]. The slabs were held at that temperature for 16 hours for proper homogenization & then air-cooled. The complete cycle of the annealing is shown in Figure1.

Since the diffusion coefficient of nickel in iron is low, nickel does not diffuse rapidly back into the core and its concentration becomes much higher at the interface than in the core. Even in relatively dilute Fe-Ni alloys, the nickel concentration just ahead of this interface can be very high. This selective oxidation of iron and concentration of nickel in a thin layer results in interpenetration of the oxide and metal at the interface and produces a tight mechanical oxide-metal bond and substantially increased oxidation resistance. The typical scale that forms on a nickel steel consists of an outer layer of mainly iron oxides, an interlayer of oxides interspersed with a largely continuous three-dimensional filigree of nickel-rich metal, every rough and indistinct oxide-metal interface, alone in which large islands of iron-rich oxides are interspersed in a matrix of nickel-rich metal, and finally an inner zone of much smaller internal oxide particles where the more reactive residues such as silicon and chromium have precipitated as oxides within the steel [1,14].

Various coatings were applied to nickel steel slabs to avoid the effect of scaling in rolled plates. Due to scaling on the surface of slab the pits & small cracks occurred in the rolled plates. The coating of "graphite powder" with sodium silicate (Na_2SiO_4) gave the better results in rolled plates as compared to coating of aluminum & redoxine [1].

The mechanical properties of nickel steel specimen such as tensile strength (1210 MPa), yield strength (1020 MPa), percent elongation (12%) were observed. High values of tensile strength, & yield strength are due to quenching & tempering of the plates in water. Percent of elongation is showing the ductility of the nickel steel plates, is due to hot working & nickel containing of steel. The hardness of the 45 mm thick plate sample quenched at 850°C was observed as (HB 366) & the hardness of the same thickness plate sample tempered at 600 °c was observed as (HB 302). The hardness of 30 mm thick plate quenched at same temperature (850°C) as 45 mm thick plate, was observed as (HB 360) & the hardness of tempered plate of same thickness at a temperature of 600 °c was observed as (HB 293). The folding tests of the nickel steel plates were also carried out & value of 120° was observed satisfactory.

The microstructure of the quenched & tempered nickel steel produced by Peoples Steel Mill (PSM) in the form of plates was observed as shown in Figures (7-10). The microstructure as shown in Figure 9 is quenched at 850°C & tempered at 600°C, was taken at 200-magnification power, showing the large grains of martensite, retained austenite & may be some amount of ferrite[2,5,14]. The microstructure as shown in Figure 10 is also quenched & tempered at same temperature, & was taken at 500--magnification power is clear than the photograph taken at 200-magnification power. The photograph taken at 700-magnification power also contains the fine martensite, retained austenite & may be some amount of ferrite [14].

4. CONCLUSIONS

1. Coating of "graphite powder" with sodium silicate ($Na_2 SiO_4$) on the surface of the slab gave the better results in rolled plates of nickel steel as compared to coating of aluminum & redoxine.

2. The mechanical properties like "Tensile strength" (1210 MPa), "Yield strength" (1020 MPa) & percent elongation (12%) were achieved during tensile tests.

3. As a result of quenching of nickel steel from 850 °c in water & tempered at 600 °C, the "Brinell hardness" (HB 366) of quenched plate of 45 mm thickness was achieved, & hardness (HB 302) of tempered plate of same thickness was achieved.

4. The "Brinell hardness" (HB 360) of quenched plate of 30 mm thickness was achieved, & hardness (HB 293) of tempered plate of same thickness was achieved at same heat treatment parameters.

5. Fine martensite structure with retained austenite was observed in the microstructure of water quenched & tempered nickel steel plate samples.

ISSN 1665-8607

CONTENTS

VOLUME 7 NO. 1 JAN-JUN 2006

1. Co-Firing of Commercial Fuel Oil and Producer Gas from Downdraft Gasifier for Industrial Applications.
Ahmad Hussain, Saleem Raza Samo and Farid Nasir Ani 1

2. Effect of Microstructural Constituents on Abrasive Wear Resistance of Carburized SAE 8822H Steel.
Muhammad Hayat Jokhio, Muhammed Ibrahim Panhwar and Mujeeb-u-ddin Memon..... 13

3. Some Steady Plane Flows of an Incompressible Newtonian Fluid
Rana Khalid Naeem, Waseem Ahmed Khan and Roohi Bano..... 19

4. A Methodology for Process Improvements Using SPC in a Continuous or Discrete Type Manufacturing Process
Abdul Sattar Jamali, Muhammad Sharif Jamali and Zameer Ahmed Abro..... 29

5. Some Exact Solutions to Equations of Motion of a Third Grade Fluid for Selected Vorticity
Rana Khalid Naeem, Waseem Ahmed Khan and Sultan Hussain..... 37

6. Nickel Steel Rolling Problems.
Muhammad Hayat Jokhio, Muhammad Ibrahim Panhwar and Moinuddin Ali Khan..... 43

Published by

Directorate of Research & Publication, Quaid-e-Awam University of Engineering, Science & Technology, Nawabshah Sindh-Pakistan
(Phone # 92-244-9370361,9370362. Fax # 92-244-9370362) email:srsamo@yahoo.com

Composed & Printed by

Soomro Computer Composers & Printers Nawabshah, Golwala Complex Katchehry Road Nawabshah
Sindh-Pakistan (Phone # 92-244-291022 Cell: 0333-7014550)